PHYSICAL REVIEW D, VOLUME 62, 072005

Measurement of $\mathcal{B}(\Lambda_c^+ \to pK^- \pi^+)$

D. E. Jaffe, G. Masek, H. P. Paar, E. M. Potter, S. Prell, and V. Sharma
University of California, San Diego, La Jolla, California 92093

D. M. Asner, A. Eppich, J. Gronberg, T. S. Hill, D. J. Lange, and R. J. Morrison
University of California, Santa Barbara, Santa Barbara, California 93106

R. A. Briere
Carnegie Mellon University, Pittsburgh, Pennsylvania 15213

B. H. Behrens, W. T. Ford, A. Gritsan, J. Roy, and J. G. Smith
University of Colorado, Boulder, Colorado 80309-0390

J. P. Alexander, R. Baker, C. Bebek, B. E. Berger, K. Berkelman, F. Blanc, V. Boisvert, D. G. Cassel, M. Dickson, P. S. Drell, K. M. Ecklund, R. Ehrlich, A. D. Foland, P. Gaidarev, L. Gibbons, B. Gittelman, S. W. Gray, D. L. Hartill, B. K. Heltsley, P. I. Hopman, C. D. Jones, D. L. Kreinick, M. Lohner, A. Magerkurth, T. O. Meyer, N. B. Mistry, C. R. Ng, E. Nordberg, J. R. Patterson, D. Peterson, D. Riley, J. G. Thayer, P. G. Thies, B. Valant-Spaight, and A. Warburton
Cornell University, Ithaca, New York 14853

P. Avery, C. Prescott, A. I. Rubiera, J. Yelton, and J. Zheng
University of Florida, Gainesville, Florida 32611

G. Brandenburg, A. Ershov, Y. S. Gao, D. Y.-J. Kim, and R. Wilson
Harvard University, Cambridge, Massachusetts 02138

T. E. Browder, Y. Li, J. L. Rodriguez, and H. Yamamoto
University of Hawaii at Manoa, Honolulu, Hawaii 96822

T. Bergfeld, B. I. Eisenstein, J. Ernst, G. E. Gladding, G. D. Gollin, R. M. Hans, E. Johnson, I. Karliner, M. A. Marsh, M. Palmer, C. Plager, C. Sedlack, M. Selen, J. J. Thaler, and J. Williams
University of Illinois, Urbana-Champaign, Illinois 61801

K. W. Edwards
Carleton University, Ottawa, Ontario, Canada K1S 5B6
and the Institute of Particle Physics, Canada

R. Janicek and P. M. Patel
McGill University, Montréal, Québec, Canada H3A 2T8
and the Institute of Particle Physics, Canada

A. J. Sadoff
Ithaca College, Ithaca, New York 14850

R. Ammar, P. Baringer, A. Bean, D. Besson, P. Brabant, M. Cervantes, I. Kravchenko, R. P. Stutz, and X. Zhao
University of Kansas, Lawrence, Kansas 66045

S. Anderson, V. V. Frolov, Y. Kubota, S. J. Lee, R. Mahapatra, J. J. O'Neill, R. Poling, T. Riehle, A. Smith, and J. Urheim
University of Minnesota, Minneapolis, Minnesota 55455

S. Ahmed, M. S. Alam, S. B. Athar, L. Jian, L. Ling, A. H. Mahmood,* M. Saleem, S. Timm, and F. Wappler
State University of New York at Albany, Albany, New York 12222

A. Anastassov, J. E. Duboscq, K. K. Gan, C. Gwon, T. Hart, K. Honscheid, D. Hufnagel, H. Kagan, R. Kass, J. Lorenc, T. K. Pedlar, H. Schwarthoff, E. von Toerne, and M. M. Zoeller
Ohio State University, Columbus, Ohio 43210

S. J. Richichi, H. Severini, P. Skubic, and A. Undrus
University of Oklahoma, Norman, Oklahoma 73019

S. Chen, J. Fast, J. W. Hinson, J. Lee, N. Menon, D. H. Miller, E. I. Shibata, I. P. J. Shipsey, and V. Pavlunin
Purdue University, West Lafayette, Indiana 47907

D. Cronin-Hennessy, Y. Kwon,† A. L. Lyon, and E. H. Thorndike
University of Rochester, Rochester, New York 14627

C. P. Jessop, H. Marsiske, M. L. Perl, V. Savinov, D. Ugolini, and X. Zhou
Stanford Linear Accelerator Center, Stanford University, Stanford, California 94309

T. E. Coan, V. Fadeyev, I. Korolkov, Y. Maravin, I. Narsky, R. Stroynowski, J. Ye, and T. Wlodek
Southern Methodist University, Dallas, Texas 75275

M. Artuso, R. Ayad, C. Boulahouache, K. Bukin, E. Dambasuren, S. Karamov, S. Kopp, G. Majumder, G. C. Moneti, R. Mountain, S. Schuh, T. Skwarnicki, S. Stone, G. Viehhauser, J. C. Wang, A. Wolf, and J. Wu
Syracuse University, Syracuse, New York 13244

S. E. Csorna, I. Danko, K. W. McLean, Sz. Márka, and Z. Xu
Vanderbilt University, Nashville, Tennessee 37235

R. Godang, K. Kinoshita,‡ I. C. Lai, and S. Schrenk
Virginia Polytechnic Institute and State University, Blacksburg, Virginia 24061

G. Bonvicini, D. Cinabro, L. P. Perera, and G. J. Zhou
Wayne State University, Detroit, Michigan 48202

G. Eigen, E. Lipeles, M. Schmidtler, A. Shapiro, W. M. Sun, A. J. Weinstein, and F. Würthwein§
California Institute of Technology, Pasadena, California 91125

(CLEO Collaboration)

(Received 28 March 2000; published 12 September 2000)

The $\Lambda_c^+ \to pK^-\pi^+$ yield has been measured in a sample of two-jet continuum events containing both a charm tag ("$\overline{D}$") as well as an antiproton ($e^+e^- \to \overline{D}\overline{p}X$), with the antiproton in the hemisphere opposite the $\overline{D}$ (measurement of charge conjugate modes is implicit throughout). Under the hypothesis that such selection criteria tag $e^+e^- \to \overline{D}\overline{p}\Lambda_c^+ X$ events, the $\Lambda_c^+ \to pK^-\pi^+$ branching fraction can be determined by measuring the $pK^-\pi^+$ yield in the same hemisphere as the antiprotons in our $\overline{D}\overline{p}X$ sample. Three types of $\overline{D}$ charm tags are used, $\pi^-_{\rm soft}$ (from $D^{*-} \to \overline{D}^0 \pi^-_{\rm soft}$), electrons (from $\overline{D} \to Xe^-\nu$), and fully reconstructed $\overline{D}^0 \to K^+\pi^-$ or $D^- \to K^+\pi^-\pi^-$ or $D_s^- \to \phi\pi^-$. Combining our results obtained from the three independent charm tags, we obtain $\mathcal{B}(\Lambda_c^+ \to pK^-\pi^+) = (5.0 \pm 0.5 \pm 1.2)\%$.

PACS number(s): 13.30.Eg, 14.20.Lq

I. INTRODUCTION

Of the four fundamental normalization branching fractions of charmed hadrons [$\mathcal{B}(D^0 \to K^-\pi^+)$, $\mathcal{B}(D^+ \to K^-\pi^+\pi^+)$, $\mathcal{B}(D_s^+ \to \phi\pi^+)$, and $\mathcal{B}(\Lambda_c^+ \to pK^-\pi^+)$],[1] the $\Lambda_c^+ \to pK^-\pi^+$ branching fraction is the least well known, and presently the most controversial. There have been two basic methods used to estimate this branching fraction. The first uses, as input, the ratio of efficiency-corrected yields $\mathcal{B}(\Lambda_c^+ \to \Lambda X l \nu)/\mathcal{B}(\Lambda_c^+ \to pK^-\pi^+)$ [1,2] and the well-measured Λ_c^+ lifetime. One can deduce a total semileptonic branching fraction for Λ_c^+ decays

$$\mathcal{B}(\Lambda_c^+ \to X l \nu) = \frac{\Gamma(\Lambda_c^+ \to X l \nu)}{\Gamma^{\rm tot}(\Lambda_c^+)},$$

assuming that the total semileptonic width is the same in Λ_c^+ decays as in $D_s^+ \to X l \nu$, $D^0 \to X l \nu$, and $D^+ \to X l \nu$ (the approximate equality of the semileptonic widths for all the

*Permanent address: University of Texas - Pan American, Edinburg, TX 78539.

†Permanent address: Yonsei University, Seoul 120-749, Korea.

‡Permanent address: University of Cincinnati, Cincinnati, OH 45221.

§Permanent address: Massachusetts Institute of Technology, Cambridge, MA 02139.

[1]Charge conjugate modes are implicit.

charmed mesons lends credence to this assumption, although mass and phase-space effects in semileptonic decays may be significant [3]), and assuming $\mathcal{B}(\Lambda_c^+ \to \Lambda X l\nu)/\mathcal{B}(\Lambda_c^+ \to X l\nu) \approx 1.0$ [4–6] [i.e., $\mathcal{B}(\Lambda_c^+ \to N\bar{K}X l\nu)/\mathcal{B}(\Lambda_c^+ \to X l\nu) \to 0$]. Under these assumptions, one can estimate the absolute branching fraction for $\Lambda_c^+ \to \Lambda X l\nu$, and, correspondingly, the absolute branching fraction for $\Lambda_c^+ \to pK^-\pi^+$ from the measured $\mathcal{B}(\Lambda_c^+ \to \Lambda X l\nu)/\mathcal{B}(\Lambda_c^+ \to pK^-\pi^+)$ yields. Such a procedure yields values in the range of $\mathcal{B}(\Lambda_c^+ \to pK^-\pi^+) \sim 6-8\%$ [6].

In the second approach, one uses the fact that baryon number must be conserved in B decay and that $\mathcal{B}(b \to c) \approx 1.0$. Under the assumption that baryon production in B decay occurs through $\bar{B} \to \Lambda_c^+ \bar{p} W$, the observed $\bar{B} \to \bar{p} X$ events provide an unbiased sample of $\bar{B} \to \Lambda_c^+ X$. Measurements of the $\Lambda_c^+ \to pK^-\pi^+$ yield in such events, therefore, allow a determination of the absolute $\Lambda_c^+ \to pK^-\pi^+$ branching fraction [4,5].[2] The Particle Data Group uses a combination of this technique and D and Λ_c^+ charm semileptonic measurements to estimate $\mathcal{B}(\Lambda_c^+ \to pK^-\pi^+) = (5.0 \pm 1.3)\%$ [7].

In this measurement, we employ a new technique to determine $\mathcal{B}(\Lambda_c^+ \to pK^-\pi^+)$ using e^+e^- annihilation continuum events. We select a sample of $e^+e^- \to c\bar{c}$ events in which a Λ_c^+ is expected to be present by requiring: (i) a charm tag consisting of either a high momentum electron, a $\pi^-_{\rm soft}$ (from $D^{*-} \to \bar{D}^0 \pi^-_{\rm soft}$), or a fully reconstructed $\bar{D}$-meson candidate and (ii) an opposite hemisphere baryon tag consisting of an antiproton. The presence of a Λ_c^+ is inferred, to compensate baryon number and charm. According to Monte Carlo simulations, the antiproton in $\overline{Dp}\Lambda_c^+$ events is as likely to have its momentum in the same hemisphere as the $\bar{D}$ as in the hemisphere opposite it. However, estimation of the non-Λ_c^+ background in our $\overline{Dp}(\Lambda_c^+)$ sample is more reliable if we require the antiproton to be in the hemisphere opposite the charm tag. We, therefore, focus on the sample in which the antiproton is in the hemisphere opposite the charm tag [''O$(\bar{p}|\bar{D})$'' events, with parentheses designating opposite hemisphere correlations].[3] Topologically, these events can be schematically depicted as:

$$
\begin{array}{ccc}
 & c \quad \bar{c} & \\
(\Lambda_c^+) \leftarrow & & \to \bar{D} \\
\bar{p} \leftarrow & &
\end{array}
$$

[2]Unfortunately, a more recent study of flavor-tagged baryon production in B decay indicates that diagrams other than $\bar{B} \to \Lambda_c^+ \bar{p} W$ may contribute substantially to Λ_c^+, $\bar{\Lambda}_c^-$, and $p/\bar{p}$ production in B decay [8].

[3]The same-hemisphere $\overline{pD}$ sample, designated with brackets as ''S$[\overline{pD}]$'' is discussed later as a cross check.

The yield of $\Lambda_c^+ \to pK^-\pi^+$ decays in this $(\bar{p}|\bar{D})$ sample will allow us, after all the appropriate corrections, to determine the branching fraction:

$$\mathcal{B}(\Lambda_c^+ \to pK^-\pi^+) = \frac{N([\bar{p}\Lambda_c^+]|\bar{D})}{N(\bar{p}|\bar{D})}.$$

Our analysis comprises two techniques – in one, we construct a three-particle correlation to determine the $\Lambda_c^+ \to pK^-\pi^+$ branching fraction, and in the second, a two-particle correlation is sufficient to infer $\mathcal{B}(\Lambda_c^+ \to pK^-\pi^+)$. In the triple correlation analysis, we take the ratio of the number of times that three particles (the Λ_c^+, antiproton, and our charm tag) are found in the same event relative to the number of times that only the antiproton and the charm tag are found. For the second technique, only a double correlation between the reconstructed Λ_c^+ and the antiproton tag constitutes the numerator of our ratio; the recoiling charm tag is assumed.

II. APPARATUS AND EVENT SELECTION

This analysis was performed using the CLEO II detector operating at the Cornell Electron Storage Ring (CESR) at center-of-mass energies $\sqrt{s} = 10.52 - 10.58$ GeV. The CLEO II detector is a general purpose solenoidal magnet spectrometer and calorimeter designed to trigger efficiently on two-photon, tau-pair, and hadronic events [9]. Measurements of charged particle momenta are made with three nested coaxial drift chambers consisting of 6, 10, and 51 layers, respectively. These chambers fill the volume from $r = 3$ cm to $r = 1$ m, with r being the radial coordinate relative to the beam $(\hat{z})$ axis. This system is very efficient $(\epsilon \geqslant 98\%)$ for detecting tracks that have transverse momenta (p_T) relative to the beam axis greater than 200 MeV/c, and that are contained within the good fiducial volume of the drift chamber $(|\cos\theta| < 0.94$, with θ defined as the polar angle relative to the beam axis). This system achieves a momentum resolution of $(\delta p/p)^2 = (0.0015p)^2 + (0.005)^2$ (p is the momentum, measured in GeV/c). Pulse height measurements in the main drift chamber provide specific ionization resolution of 5.5% for Bhabha events, giving good K/π separation for tracks with momenta up to 700 MeV/c and separation of order 2σ in the relativistic rise region above 2 GeV/c. Outside the central tracking chambers are plastic scintillation counters, which are used as a fast element in the trigger system and also provide particle identification information from time-of-flight measurements.

Beyond the time-of-flight system is the electromagnetic calorimeter, consisting of 7800 thallium-doped CsI crystals. The central ''barrel'' region of the calorimeter covers about 75% of the solid angle and has an energy resolution which is empirically found to follow

$$\frac{\sigma_{\rm E}}{E}(\%) = \frac{0.35}{E^{0.75}} + 1.9 - 0.1E;$$

E is the shower energy in GeV. This parametrization includes effects such as noise, and translates to an energy resolution of about 4% at 100 MeV and 1.2% at 5 GeV. Two end-cap regions of the crystal calorimeter extend solid angle coverage to about 95% of 4π, although energy resolution is not as good as that of the barrel region. The tracking system, time-of-flight counters, and calorimeter are all contained within a superconducting coil operated at 1.5 T. Flux return and tracking chambers used for muon detection are located immediately outside the coil and in the two end-cap regions.

The event sample used for this measurement is comprised of 3.1 fb^{-1} of data collected at the $\Upsilon(4S)$ resonance and 1.6 fb^{-1} of data collected about 60 MeV below the $\Upsilon(4S)$ resonance. Approximately 5×10^6 continuum $c\bar{c}$ events are included in this sample.

Event selection criteria

In order to suppress background and enrich the hadronic fraction of our event sample, we impose several event requirements. Candidate events must have: (1) at least four detected, good quality, charged tracks; (2) an event vertex consistent with the known e^+e^- interaction point; (3) a total measured visible event energy, defined as the sum of the measured energy carried by charged tracks plus the measured energy carried by neutral particles ($E_{\mathrm{vis}}=E_{\mathrm{chrg}}+E_{\mathrm{neutral}}$) greater than 110% of the single beam energy, $E_{\mathrm{vis}}>1.1\cdot E_{\mathrm{beam}}$. In addition, when using an electron to tag a $c\bar{c}$ event we require that either the beam energy E_{beam} be less than 5.275 GeV [below the $\Upsilon(4S)\to B\bar{B}$ threshold] or that the event be well collimated. Specifically, the ratio of Fox-Wolfram event shape parameters $H2/H0$ can be used to quantify the ''jettiness'' of an event [10] — for a perfectly spherical flow of event energy, this ratio equals 0; for a perfectly jetty event, this ratio equals 1.0. For our electron tags, we require this ratio to be greater than 0.35. This final requirement helps remove contamination from semileptonic B decays in $B\bar{B}$ events. (The correlation between the soft pion momentum vector and the thrust axis is absent in $B\bar{B}$ events, therefore $B\bar{B}$ events do not contribute to our soft pion-tagged event sample.)

III. TAG IDENTIFICATION

A. Charm tags

For our analysis, we select continuum hadronic events which, in addition to an antiproton, contain either a high momentum electron (from $\bar{D}\to Xe\nu$), a π^-_{soft} (from $D^{*-}\to\bar{D}^0\pi^-_{\mathrm{soft}}$), or a fully reconstructed $\bar{D}$-meson candidate as a charm tag (''$\bar{D}$'') of $e^+e^-\to c\bar{c}$ events. Since the different tags have different systematic uncertainties and procedures associated with them, we now discuss separately the various tags employed in this measurement, beginning with our electron charm tags.

1. Electron tags

To suppress background from fake electrons, as well as true electrons not necessarily associated with charm decays in $e^+e^-\to c\bar{c}$ events, we require that our electron-tag candidates satisfy the following criteria:

(a) The electron must pass a strict ''probability of electron'' identification criterion. This identification likelihood combines measurements of a given track's specific ionization deposition in the central drift chamber with the ratio of the energy of the associated calorimeter shower to the charged track's momentum [11]. True electrons have shower energies approximately equal to their drift chamber momenta; hadrons tend to be minimum ionizing and have considerably smaller values of shower energy relative to their measured momenta. We require that the logarithm of the ratio of a charged track's electron probability relative to the probability that the charged track is a hadron be greater than 7.0. In the good fiducial volume of the CLEO detector ($|\cos\theta|<0.7$, where θ is the track's polar angle measured relative to the e^+e^- beam axis), the efficiency of this requirement is $>90\%$ in our momentum interval of interest; the likelihood of a nonelectron faking an electron is less than 1%. The total electron fake fraction is thus the product of the fake rate per track times the typical charged track multiplicity and is therefore not large ($\leqslant10\%$).

(b) The momentum of the electron must be greater than 1 GeV/c. This criterion helps eliminate fake electrons due to kaon and pion tracks and also suppresses electrons from photon conversions ($\gamma\to e^+e^-$) and π^0 Dalitz decays ($\pi^0\to\gamma e^+e^-$).

(c) The electron must have an impact parameter (''DOCA,'' or distance-of-closest-approach) relative to the primary event vertex of less than 4 mm along the radial coordinate and no more than 2 cm along the beam axis. This provides additional suppression of electrons resulting from photon conversions.

2. Soft-pion tags

Our soft-pion tag candidates must pass the following restrictions:

(a) The pion must have an impact parameter relative to the event vertex of less than 5 mm along the radial coordinate and no more than 5 cm along the beam axis.

(b) The pion must pass a 99% probability criterion for pion identification, based on the associated specific ionization collected in the drift chamber.

(c) The pion's momentum must lie between 0.15 GeV/c and 0.40 GeV/c.

(d) The pion's trajectory must lie near the trajectory of the parent charm quark, as expected for pions produced in $D^{*-}\to\bar{D}^0\pi^-_{\mathrm{soft}}$. Experimentally, this is checked using the variable $\sin^2\theta$, where θ is the opening angle between the candidate soft pion and the event thrust axis [12]. Assuming that the thrust axis approximates the original $c\bar{c}$ axis, true π^-_{soft} should populate the region $\sin^2\theta\to0$. Figure 1 displays the soft pion $\sin^2\theta$ distribution for candidates passing our event and track selection criteria. The excess in the region $\sin^2\theta\to0$ constitutes our charm-tagged sample.

3. $\bar{D}^0$, D^-, and D_s^- tags

Fully reconstructed $\bar{D}$-meson tags are detected in the modes $\bar{D}^0\to K^+\pi^-$, $D^-\to K^+\pi^-\pi^-$, and $D_s^-\to\phi\pi^-$. In

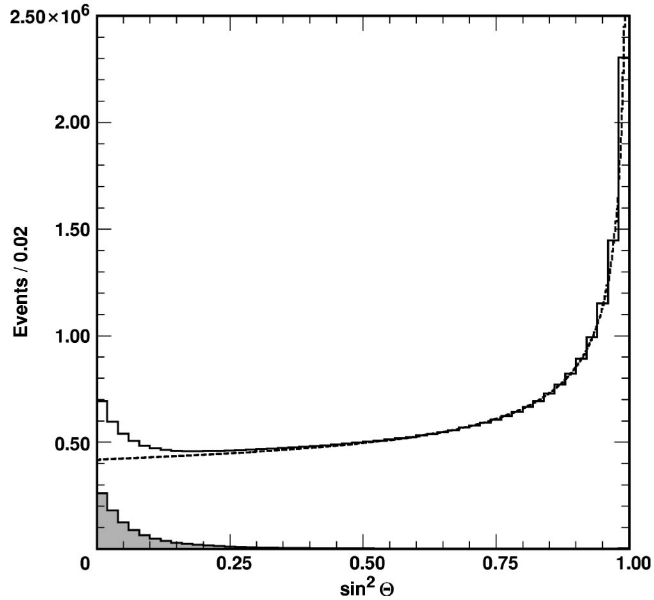

FIG. 1. Shown is the inclusive $\sin^2\theta$ distribution for all tracks (solid histogram) overlaid with the background fit function (dashed) and the $\pi^-_{\rm soft}$ signal expected from $D^{*-}\to\bar{D}^0\pi^-_{\rm soft}$ decays (shaded). Determination of signal and background follows an earlier CLEO analysis [12], which used this method to measure $\mathcal{B}(D^0\to K^-\pi^+)$.

all cases, final-state particles are required to pass DOCA criteria with respect to the primary vertex in both the radial ($|\mathrm{DOCA}|<5$ mm) and beam ($|\mathrm{DOCA}|<5$ cm) coordinates. Final-state particles are also required to have specific ionization and time-of-flight information consistent with their assumed identities.

B. Antiproton tags

To be considered as candidates for antiproton (or proton, in the charge conjugate case) ''tags,'' charged particles detected in the central drift chamber must also pass strict particle identification criteria. Using the available time-of-flight and drift chamber specific ionization measurements for each track, the likelihood that a particle be an antiproton must be at least nine times larger than the likelihood that the particle be a K^- or a π^-. Antiproton tag candidates must also pass the same vertex requirements as soft pion and electron candidates. These vertex criteria help suppress backgrounds from nonprimary antiprotons (from $\bar{\Lambda}\to\bar{p}\pi^+$, e.g.) or baryons generated by collisions of beam particles with either the beampipe itself or residual gas within the beampipe.

It is important that our antiproton tags be direct, and not hyperon daughters. By combining our antiproton candidates with remaining charged tracks in the same event (assumed to be pions), we can reconstruct $\bar{\Lambda}$'s and estimate the fraction of our antiproton tags which are due to reconstructed $\bar{\Lambda}$'s decay. We determine this fraction to be $<2\%$ (Sec. IV A 3).

We check the fraction of our proton tags originating in beam-gas and beam-wall collisions by determining the asymmetry between the number of proton tags and antiproton tags. If the beam-gas/beam-wall contamination is large, we expect there to be a preponderance of proton tags compared to antiproton tags. In fact, in a $\bar{D}$-meson tagged subset of the full data used in this analysis, we find the number of proton tags (6980 ± 255) to be statistically equal to the number of antiproton tags (6737 ± 250). Nevertheless, the difference between these two numbers is taken as our systematic uncertainty in the magnitude of beam-related backgrounds (Table II).

IV. TRIPLE CORRELATIONS

In the triple correlation analysis, we tag the $\bar{c}$ side of an $e^+e^-\to c\bar{c}$ event using a soft pion or an electron tag, then search for a $\bar{p}$ in the opposite hemisphere. In order to conserve both charm and baryon number we assume a Λ_c^+ in the hemisphere opposite the tag. Below we show a schematic diagram of an event where either a $\pi^-_{\rm soft}$ or e^-, in combination with an anti-proton, is used to tag an unseen (Λ_c^+) decay.

$c \quad \bar{c}$

$\bar{p} \hookleftarrow$ $\qquad\qquad \hookrightarrow D^{*-}$

$(\Lambda_c^+)\hookleftarrow$ $\qquad\qquad \hookrightarrow \bar{D}^0\pi^-_{\rm soft}$

$(\text{anything})\hookleftarrow$ $\qquad\qquad \hookrightarrow e^-K^+\nu_e$

The above diagram gives us a known sample of Λ_c^+ events. (Note that we do not require that both $\pi^-_{\rm soft}$ and e^- tags be present in a candidate event; the presence of either one constitutes a valid ''charm tag.'') In the electron tag case, the total number of Λ_c^+'s is the number of events in which a track passes our electron tag identification and an antiproton tag is found in the opposite hemisphere. We then reconstruct, in that sample, a Λ_c^+ decaying into $pK^-\pi^+$ in the same hemisphere as the $\bar{p}$, and opposite the electron candidate. The Λ_c^+ invariant mass distribution is then fit to a first order Chebyschev polynomial to represent the background and a Gaussian to represent the signal (Fig. 2), with the Λ_c^+ mass and width fixed to the values obtained from a fit to the inclusive Λ_c^+ mass spectrum in data.

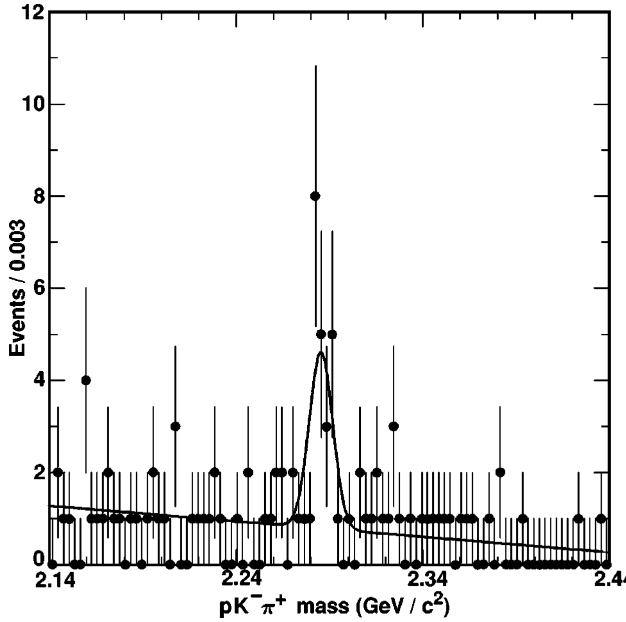

FIG. 2. The candidate Λ_c^+ mass (i.e., $pK^-\pi^+$ mass, in GeV/c^2) for Λ_c^+'s with a $\overline{p}$ in the same hemisphere $[\Lambda_c^+\overline{p}]$ and an e^- in the opposite hemisphere ($\Lambda_c^+ e$). The triple correlation yield is 10.3 ± 3.8 events.

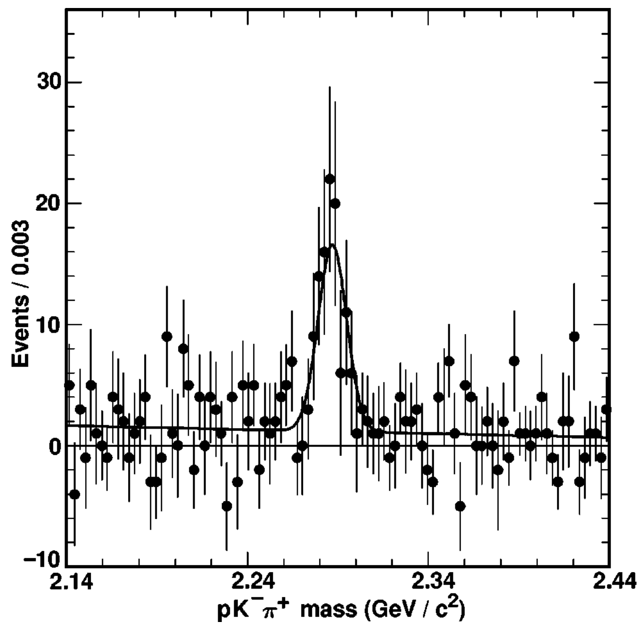

FIG. 3. Results of sideband subtraction in data to determine $\Lambda_c^+\to pK^-\pi^+$ yield in soft-pion tagged events. We project onto the candidate Λ_c^+ mass axis the portion of our two-dimensional $pK^-\pi^+$ mass vs $\sin^2\theta$ plot corresponding to $\sin^2\theta<0.25$ and subtract the scaled projection corresponding to $0.25\leqslant\sin^2\theta\leqslant 0.5$. We then perform a fit to the resulting $pK^-\pi^+$ mass spectrum in order to find our final yield of $c\overline{c}\to\Lambda_c^+ + \overline{p} + \pi^-_{\rm soft} + X$ events. The raw triple correlation yield is 101.6 ± 20.6 events.

When using the soft pion tag, we select events that are supposed to contain a Λ_c^+ by plotting the $\sin^2\theta$ distribution of pions having a tag $\overline{p}$ in the opposite hemisphere, with θ defined as before as the angle between the pion's momentum and the thrust axis (Fig. 1). Background and signal distributions are then fit to this $\sin^2\theta$ distribution. The background function we use is $f(x)=C_1(1/\sqrt{1-x})+C_2(1/\sqrt{1+Ax^2+Bx^3})$, where x is $\sin^2\theta$. This functional form is taken from a previous CLEO measurement of $\mathcal{B}(D^0\to K^-\pi^+)$ using a similar technique [13].

Using the soft pion tag, we extract the number of signal events from a two-dimensional plot of $pK^-\pi^+$ invariant mass versus the $\sin^2\theta$ of the $\pi^-_{\rm soft}$. From this two-dimensional distribution, we perform a scaled sideband subtraction of the Λ_c^+ yield in the "sideband" region ($0.25<\sin^2\theta<0.5$) compared with the signal region ($\sin^2\theta<0.25$) to determine the final, background-subtracted yield (Fig. 3). (The background is approximately linear through this region.) We have compared the yield obtained this way with the yield obtained using the $\sin^2\theta$ signal remaining after Λ_c^+-mass sideband subtraction (91 ± 18 events). The two techniques give consistent results; the difference between them is counted towards the final systematic error (Table II).

For both tags, we can now quantify the ratio of tagged events containing a Λ_c^+ decaying into $pK^-\pi^+$ to all tagged events. This ratio is equal to

$$R=\frac{\mathcal{Y}[e^+e^-\to\overline{D}+\overline{p}+(\Lambda_c^+\to pK^-\pi^+)+X]}{\mathcal{Y}(e^+e^-\to\overline{D}+\overline{p}+X)},\qquad(1)$$

where $\mathcal{Y}$ stands for yield in e^+e^- annihilation, $\overline{D}$ designates any one of our charm tags, and the $\overline{p}$ and the $\overline{D}$ are in opposite hemispheres with respect to the thrust axis of the event.

Now the numerator can be written as

$$\begin{aligned}\mathcal{Y}[e^+e^-&\to\overline{D}+\overline{p}+(\Lambda_c^+\to pK^-\pi^+)+X]\\&=\mathcal{L}\cdot\sigma(e^+e^-\to c\overline{c})\cdot\mathcal{B}(c\overline{c}\to\overline{D}+\overline{p}\\&\quad+\Lambda_c^++X)\cdot\mathcal{B}(\Lambda_c^+\to pK^-\pi^+)\cdot(\epsilon_{\overline{D}})\cdot(\epsilon_{\overline{p}})\cdot(\epsilon_{\Lambda_c^+})\end{aligned}\qquad(2)$$

and the denominator

$$\begin{aligned}\mathcal{Y}[e^+e^-\to\overline{D}+\overline{p}+X]&=\mathcal{L}\cdot\sigma(e^+e^-\to c\overline{c})\cdot\mathcal{B}(c\overline{c}\to\overline{D}+\overline{p}\\&\quad+\Theta_c+X')\cdot(\epsilon_{\overline{D}})\cdot(\epsilon_{\overline{p}}),\end{aligned}\qquad(3)$$

where Θ_c is any charm+baryon system, not necessarily a Λ_c^+ (e.g. it could be a D + nucleon or a charmed baryon, such as a Ξ_c, not always decaying into Λ_c^++X), $\mathcal{L}$ is the total luminosity, and $\epsilon_{\overline{p}}$, $\epsilon_{\Lambda_c^+}$, and $\epsilon_{\overline{D}}$ are the efficiencies of finding the antiproton, Λ_c^+, and charm tags, respectively.

We then write

$$\mathcal{Y}(e^+e^- \to \overline{D} + \overline{p} + X) = f_1 \cdot \mathcal{L} \cdot \sigma(e^+e^- \to c\overline{c}) \cdot \mathcal{B}(c\overline{c} \to \overline{D} + \overline{p} + \Lambda_c^+ + X) \cdot \epsilon_{\overline{D}} \cdot \epsilon_{\overline{p}}, \quad (4)$$

where

$$f_1 \equiv \frac{\mathcal{B}(c\overline{c} \to \overline{D} + \overline{p} + \Theta_c + X')}{\mathcal{B}(c\overline{c} \to \overline{D} + \overline{p} + \Lambda_c^+ + X)}. \quad (5)$$

Since f_1 takes into account the fact that our yield includes also charmed, baryonic systems other than Λ_c, $f_1 \geqslant 1.0$. Then,

$$\mathcal{B}(\Lambda_c^+ \to pK^-\pi^+) = \frac{R \cdot f_1}{\epsilon_{\Lambda_c^+}}. \quad (6)$$

Since the above equation holds for both data and Monte Carlo simulations we can write:

$$\frac{\mathcal{B}(\Lambda_c^+ \to pK^-\pi^+)_{Data}}{\mathcal{B}(\Lambda_c^+ \to pK^-\pi^+)_{MC}} = \frac{R_{Data} \cdot \epsilon_{\Lambda_c^+(MC)} \cdot f_{1(Data)}}{R_{MC} \cdot \epsilon_{\Lambda_c^+(Data)} \cdot f_{1(MC)}}. \quad (7)$$

We use Monte Carlo simulations to determine event and particle reconstruction efficiencies. The simulated sample size corresponds to approximately 6 fb^{-1} of integrated luminosity. Our Monte Carlo simulation combines an $e^+e^- \to c\overline{c}$ event generator (JETSET 7.3 [14]) with a GEANT-based [15] simulation of our detector. Assuming that the detector simulation accurately reproduces the efficiency of reconstructing a Λ_c^+ in a tagged event and that we can determine the correction f_1 in both data and Monte Carlo simulations, we can then calibrate our observed value of Λ_c^+ per tagged event in data to Monte Carlo simulations:

$$\frac{f_{1,Data}}{f_{1,MC}} \frac{R_{Data}}{R_{MC}} \cdot \mathcal{B}(\Lambda_c^+ \to pK^-\pi^+)_{MC} = \mathcal{B}(\Lambda_c^+ \to pK^-\pi^+)_{Data}. \quad (8)$$

A. Purity of our event sample

We seek, wherever possible, to measure backgrounds directly from data and thereby minimize the Monte Carlo dependence; i.e., we prefer to measure $f_{1(Data)}$ and $f_{1(MC)}$ separately rather than to assume equality of these fractions. According to event simulations, the primary non-Λ_c^+ contribution to the numerator of f_1 is due to events where baryon number opposite the $\overline{p}$ tag is conserved by another nucleon and a D meson is created in the hemisphere opposite our anticharm ("$\overline{D}$") tag, so that no Λ_c^+ is present in the event. We refer to these events as $D\overline{D}N\overline{p}$ events. In order to estimate the number of $D\overline{D}N\overline{p}$ events that contaminate our tagged event sample, we measure the number of events containing a $\overline{p}$ tag and a D meson in the same hemisphere (S[$\overline{p}D$], see Fig. 4) and assume (without reconstructing) a $\overline{D}$ in the opposite hemisphere to conserve charm. A correction ($11 \pm 2\%$ in data, described in Secs. IV A and V B 1 of this document) is made to $\mathcal{B}(\Lambda_c^+ \to pK^-\pi^+)$ based on the observed yields of these $D\overline{D}N\overline{p}$ events in data and Monte Carlo simulations. A much smaller contribution to f_1 arises from $\Xi_c X \overline{D}\overline{p}$ (also discussed later in the text).

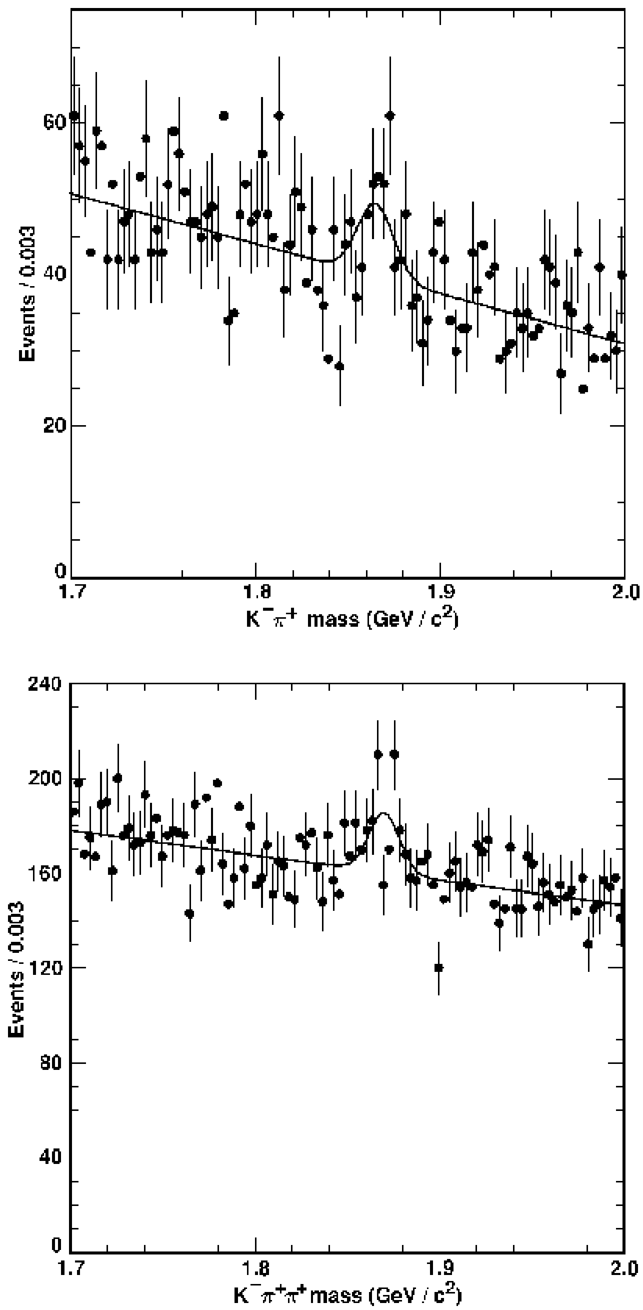

FIG. 4. Candidate D^0 (top) and D^+ (bottom) mass (GeV/c^2) for D candidates in the same hemisphere as a $\overline{p}$ [$D\overline{p}$]. Events in the D signal region are $D\overline{D}N\overline{p}$ events that contaminate our candidate Λ_c^+ event sample. The masses and widths of the D^0 and D^+ are taken from fits to the inclusive mass spectra in data.

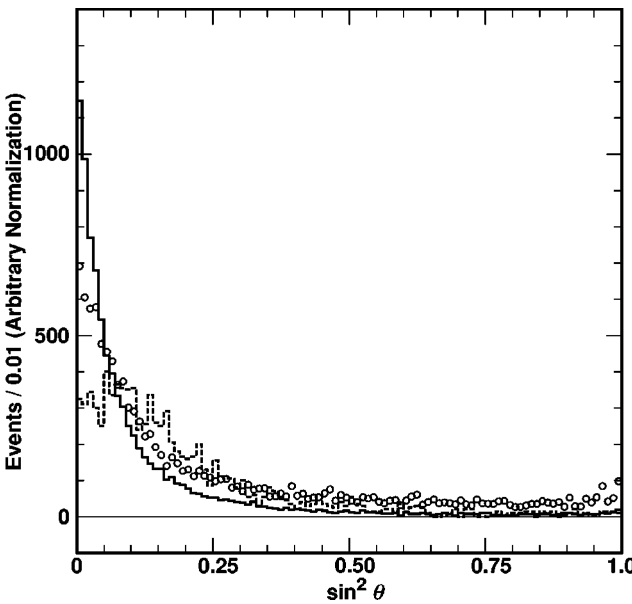

FIG. 5. Monte Carlo $\sin^2\theta$ distribution of π^-'s from $D^{*-}\to D^0\pi^-$ (solid line), $\Lambda_{cJ}^+(2593)\to\Lambda_c^+\pi^+\pi^-$ (diamonds), and $\Sigma_c^0\to\Lambda_c^+\pi^-$ (dashed line) after all event and particle identification cuts are applied to the π^-'s.

Antiprotons from $\overline{\Lambda}_c$ decay entering the hemisphere of the D meson and $\overline{\Lambda}_c p \overline{D}$ events must not be large in order for our assumption that the $S[D\overline{p}]$ sample can be used to estimate the level of $D\overline{D}N\overline{p}$ background be valid. In order to check for antiprotons from $\overline{\Lambda}_c$'s decaying into the hemisphere of a D, we plot the cosine of the angle between the antiproton's momentum vector and its parent $\overline{\Lambda}_c$. For antiprotons passing our event and track criteria, back hemisphere leakage is found to be negligible ($<1\%$). Events containing $\overline{\Lambda}_c p \overline{D}$ must contain two baryon-antibaryon pairs as well as a charmed meson (e.g., $\overline{\Lambda}_c^- \overline{p} NND$). Although it is possible to have four baryons and a charmed meson in the same event it should be noted that this process would lead to an overestimation of our background (i.e., events that contain a $D\overline{p}$ but do not tag $D\overline{D}N\overline{p}$ events), thus biasing us towards a $\mathcal{B}(\Lambda_c^+\to pK^-\pi^+)$ that is higher than the true branching fraction. Monte Carlo simulations indicate that this background is exceedingly ($<1\%$) small.

1. Contamination of the π_{soft}^- sample

Pions from $\Sigma_c^0\to\Lambda_c^+\pi^-$ and orbitally excited $\Lambda_{cJ}^+\to\Lambda_c^+\pi^+\pi^-$ decays have $\sin^2\theta$ distributions similar to the soft pions from D^{*-} decays as seen in Fig. 5. Although the number of Σ_c^0 and Λ_{cJ}^- particles [primarily $\Lambda_c^-(2593)$ and $\Lambda_c^-(2630)$] is small relative to the number of D^{*-} particles, this background is potentially significant since the likelihood for having a $\overline{p}$ tag is large in events containing these charmed baryons. In order to estimate the magnitude of these events in data and Monte Carlo simulation we perform a fit using Monte Carlo derived $\sin^2\theta$ distributions for tagged $\pi_{\rm soft}^-$ decaying from both D^{-*} and Σ_c^0 decays. We fit these distributions to our plot of the inclusive $\pi_{\rm soft}^-\sin^2\theta$ spectrum in events containing a $\overline{p}$ in the hemisphere opposite the $\pi_{\rm soft}^-$ with respect to the thrust axis (see Fig. 6). The difference between the data and Monte Carlo simulation $(\Sigma_c+\Lambda_{c,J})$ $\pi_{\rm soft}^-$ fit fractions relative to the total $\pi_{\rm soft}^-$ yield in data (14

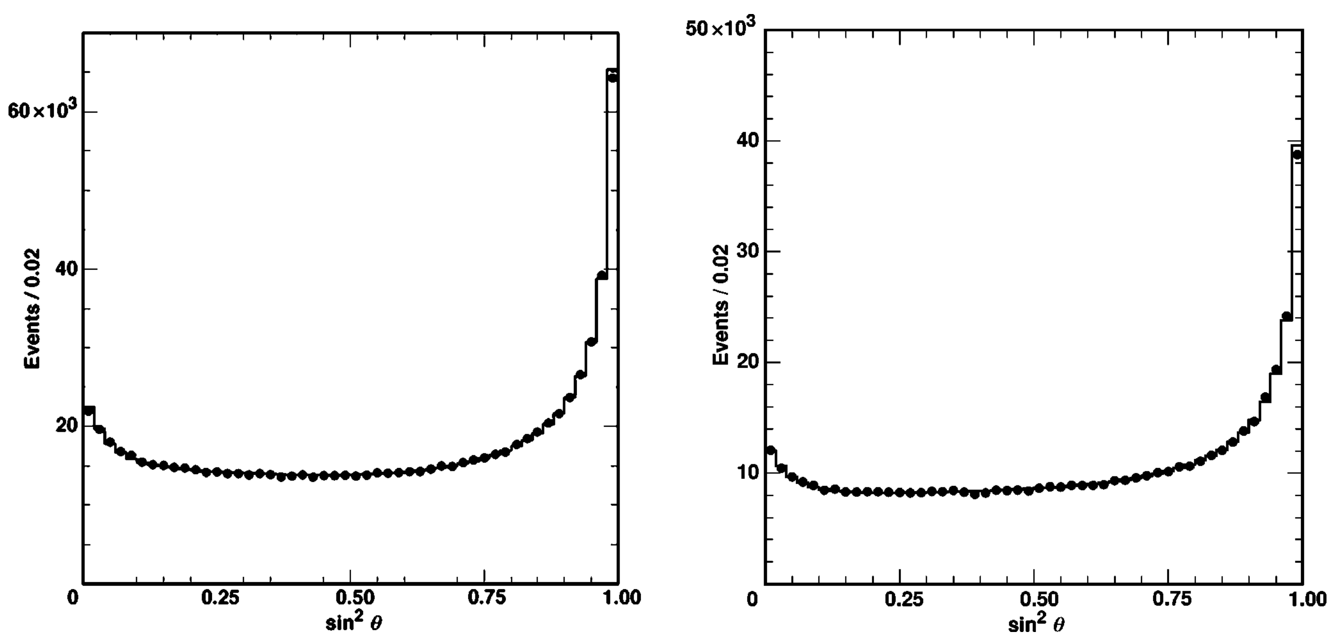

FIG. 6. $\sin^2\theta$ distribution of π^-'s in data events containing a tag antiproton in the opposite hemisphere $O(\pi_{\rm soft}^-|\overline{p})$, for Monte Carlo simulations (left) vs data (right). A free fit is performed using the Monte Carlo $\sin^2\theta$ distributions for π^-'s decaying from $D^{*-}\to D^0\pi^-$, $\Sigma_c^0\to\Lambda_c^+\pi^-$, and $\Lambda_c(2593)\to\Lambda_c^+\pi^+\pi^-$. This plot is made after all event and $\pi_{\rm soft}^-$ particle identification cuts have been applied. The fitted $\Sigma_c+\Lambda_{cJ}$ fractions for Monte Carlo simulations and data are $21\pm9\%$ and $14\pm17\%$, respectively.

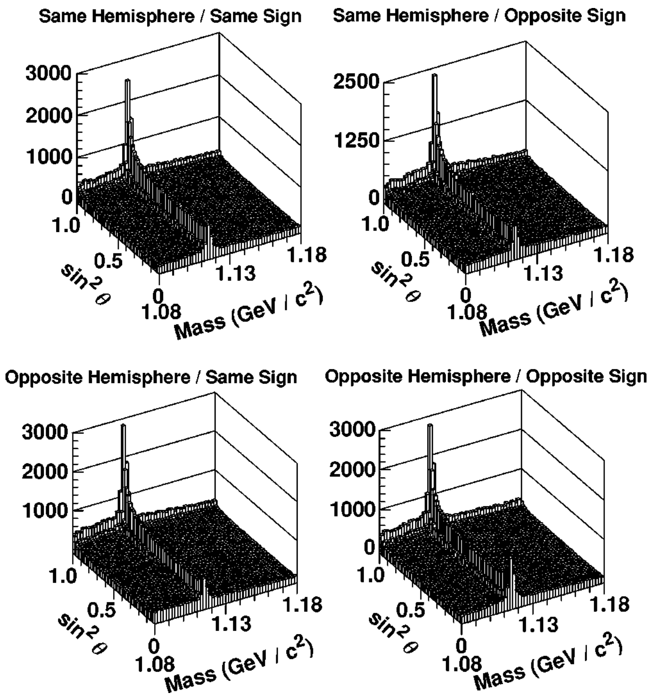

FIG. 7. Candidate $\overline{\Lambda}$ mass versus the $\sin^2\theta$ of tag $\pi^-_{\rm soft}$ in the opposite hemisphere in data $O(\overline{\Lambda}|\pi^-_{\rm soft})$. The lower left-hand plot is the hemisphere and sign correlation (opposite hemisphere/same sign) of interest. We use this plot to check for an excess of $([\Xi_c\overline{\Lambda}]|D^{*-})$ events in data as compared to Monte Carlo simulations. The excess of candidate signal events at $\sin^2\theta \to 0$ and $m_{\bar{p}\pi^-} \sim m_\Lambda$ in the lower right-hand plot is attributed to $O(\Lambda_c^+|D^{*-})$ events, in which $\Lambda_c^+ \to \Lambda X$.

$\pm 17)\%$ as compared to the Monte Carlo simulation $(21 \pm 9)\%$[4] is taken as a systematic error (Table II).

2. Electron tag backgrounds

We assume that our tag electrons are not only true electrons in $c\overline{c}$ events, but also that they are coming from semileptonic charm decay. In Monte Carlo simulations $\sim 87\%$ of our tag electrons are true electrons coming from charm semileptonic decays. The remainder of our tag electrons are either background fakes (i.e., nonelectrons) or background electrons not from charm decays (predominantly from the decay $\pi^0 \to e^+e^-\gamma$). Each of these backgrounds contributes approximately equally to our candidate electron sample. The number of fake electron tags should cancel in our equation for $\mathcal{B}(\Lambda_c^+ \to pK^-\pi^+)$, unless there is a decreased probability of tag electron fakes in events that contain a $\Lambda_c^+\overline{p}$ as compared to those only containing a $\overline{p}$. Since this very well may be the case, we vary the electron identification cuts and take the change in the calculated $\mathcal{B}(\Lambda_c^+ \to pK^-\pi^+)$ as a systematic error (5%, as listed in Table II).

Another possible source of tag electron background is from two-photon annihilations, in which one of the incident beam particles scatters into the detector. The two-photon contamination is assessed by determining the asymmetry between the number of positrons in the forward hemisphere compared to the number of electrons in the negative hemisphere (beam positrons define $+\hat{z}$ in the local coordinate system). We find two-photon annihilations to be negligible $(<1\%)$ in our tag electron sample.

[4]The actual fraction in Monte Carlo simulation is 12%.

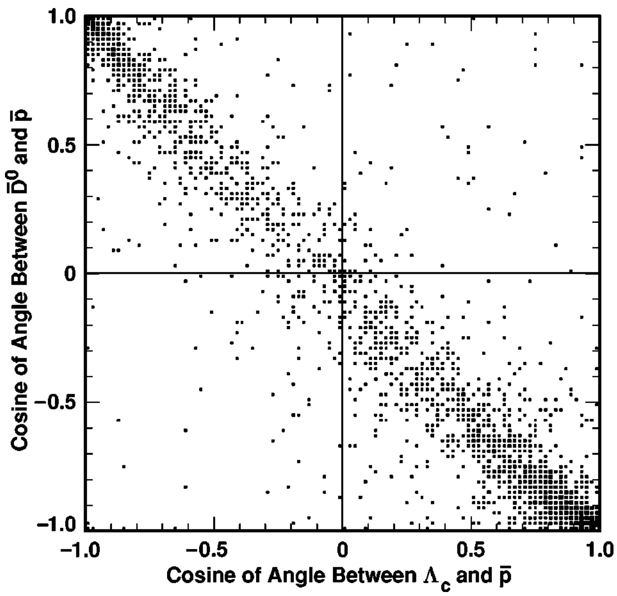

FIG. 8. Cosine of the angle between the tag antiproton momentum vector and Λ_c^+ momentum vector (horizontal) versus cosine of the angle between the tag antiproton momentum and $\overline{D}^0$ momentum (vertical) in $\Lambda_c^+\overline{D}^0\overline{p}$ events from Monte Carlo simulations, with no particle cuts (i.e., minimum momentum and track reconstruction cuts, etc.) applied. Events in the lower-left-hand quadrant are due primarily to $c\overline{c}g$ and $c\overline{c}\gamma$ events. In these events we have an antiproton that passes our tag antiproton cuts but is in the opposite hemisphere of both a Λ_c^+ and a $\overline{D}^0$, thus giving us a slight excess $(\sim 2\%)$ of $\overline{D}^0$ opposite $\overline{p}$ events relative to $\Lambda_c^+\overline{p}$ same hemisphere events. The lower-right-hand quadrant corresponds to our signal events. The upper-left hand quadrant event sample is used later for a cross check (Sec. V D).

3. Backgrounds from $([\Xi_c\overline{\Lambda}]|\overline{D})$

Tagged events may also contain a charmed baryon other than a Λ_c^+; most likely a Ξ_c. It is, therefore, important to check that the ratio of Ξ_c/Λ_c^+ production rates is similar in data and Monte Carlo simulations. Monte Carlo simulations (JETSET 7.3) indicate that, in events passing our event selection criteria, and having an antiproton tag originating from the primary vertex, $\Xi_c/\Lambda_c^+ = 0.014$. Since this fraction is so small in Monte Carlo simulations, the data fraction must be inconsistent with the Monte Carlo expectation by at least an order of magnitude to make a significant difference in our calculation of $\mathcal{B}(\Lambda_c^+ \to pK^-\pi^+)$. In order to check the fraction of our tagged event sample containing a Ξ_c instead of a Λ_c^+, we plot the $\sin^2\theta$ of $\pi^-_{\rm soft}$ versus the mass of an opposite hemisphere $\overline{\Lambda}$ (Fig. 7), rather than an opposite hemisphere $\overline{p}$.

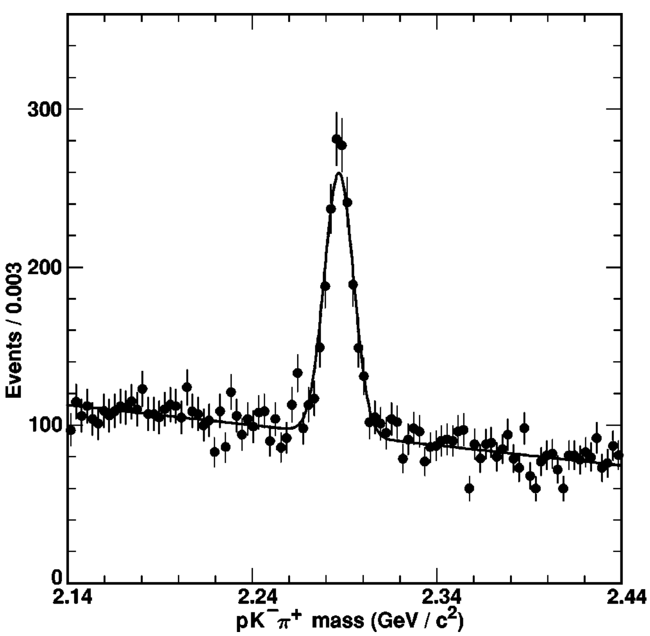

FIG. 9. Candidate Λ_c^+ mass (i.e., $pK^-\pi^+$ mass, in GeV/c^2) for Λ_c^+'s with a $\overline{p}$ in the same hemisphere S[$\overline{p}\Lambda_c^+$]. In these events a $\overline{D}$ meson is assumed to recoil in the hemisphere opposite the Λ_c^+: O($\overline{D}|\Lambda_c^+$).

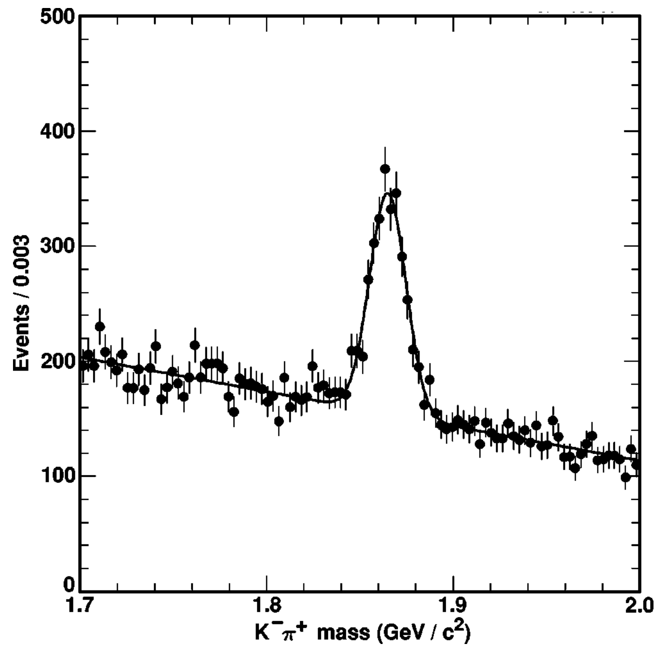

FIG. 10. Candidate $\overline{D}^0$ mass (i.e., $K^+\pi^-$ mass, in GeV/c^2) with a $\overline{p}$ in the opposite hemisphere O($\overline{D}|\overline{p}$). In these events a Λ_c^+ is assumed to exist in the hemisphere opposite the $\overline{D}^0$: O($\overline{D}^0|\Lambda_c^+$).

This is not the correct sign correlation for $\overline{\Xi}_c \to \overline{\Lambda}$ decays since the $\pi^-_{\rm soft}$ tags a D^{*-} (such a correlation implies $\overline{c}$ in both hemispheres). Instead, we assume that the dominant contributor to this plot is from $\overline{\Lambda}$'s conserving baryon number with a same hemisphere Ξ_c [i.e. ($[\Xi_c\overline{\Lambda}]|D^{*-})X$ events]. Although other O($\overline{\Lambda}|\overline{D}$) topologies may contribute (e.g., $\overline{D}^0\overline{\Lambda}K^-N$), it is still probable that an excess of Ξ_c production in our $\pi^-_{\rm soft}$ event sample would be noticed as an excess in $\overline{\Lambda}$ production opposite our tag $\pi^-_{\rm soft}$. In fact we do not see this excess; we find $(1.3\pm0.2)\times10^{-3}\overline{\Lambda}$ per $\pi^-_{\rm soft}$ tagged event in data vs $(1.6\pm0.2)\times10^{-3}$ in Monte Carlo simulations. (Note that we have already suppressed $\Xi_c\overline{\Lambda}D^{*-}$ events by requiring the tag antiproton to come from the primary event vertex.) These checks do not however address a possible excess of $\Xi_c\overline{p}KD^{*-}$ events. In principle, one could estimate Ξ_c/Λ_c in data by reconstructing Ξ_c's in the hemisphere of a tag antiproton. However, we are unable to make an accurate estimate of the $\Xi_c\overline{p}$ yield due to low reconstruction efficiency. Therefore, using the similarity of the relative $\overline{\Lambda}/\pi^-_{\rm soft}$ production ratio in data vs Monte Carlo simulations as guidance, we assume the same Ξ_c/Λ_c production ratio in data as in Monte Carlo simulations. It should be noted that although the systematic error assessed due to uncertainties in Ξ_c production is small (3%, see Table II), this magnitude of systematic error represents twice the amount of Ξ_c production predicted by Monte Carlo simulations for our tagged event sample.

B. Hemisphere correlation

There is an additional systematic error due to the hemisphere correlation requirements we impose on the $(\overline{p}|\overline{D})$ and $[\overline{p}\Lambda_c^+]$ samples. In fact, not all $\overline{pD}\Lambda_c^+$ events in which the $\overline{pD}$ are in opposite hemispheres necessarily have the $\overline{p}\Lambda_c^+$ in the same hemisphere (e.g., if the three momentum vectors have opening angles of 120° between them). This can happen in events with photon or gluon radiation. For $c\overline{c}g$ or $c\overline{c}\gamma$ (initial state radiation) events, the $c\overline{c}$ will not be directly back to back. This can be seen in Fig. 8, which shows the $\overline{pD}$ opening angle vs the $\overline{p}\Lambda_c^+$ opening angle for Monte Carlo $\overline{pD}\Lambda_c^+$ events. Note that, in producing this distribution, we have not required that either the $\overline{D}$ or Λ_c^+ be high momentum, as we would for our standard data analysis, whereas the momenta for charm particles in radiative $c\overline{c}$ events is typically smaller. Nevertheless, the fraction of $\Lambda_c^+\overline{pD}$ events in which the antiproton is found in the lower-left quadrant of Fig. 8 is taken as a systematic error (Table II), reflecting the fact that the hemisphere correlation is not rigorous, and that these angular distributions may be different in data vs Monte Carlo simulation.

V. DOUBLE CORRELATIONS

A. Method

In order to circumvent the low statistics involved with the triple correlation methods we exploit a double correlation method. We begin with events containing a S[$\overline{p}\Lambda_c^+$] in the same hemisphere. In these events a $\overline{c}$ hadron can be assumed in the hemisphere opposite the Λ_c^+. According to Monte Carlo simulations, this $\overline{c}$ hadron will most likely be an anticharmed meson. Events containing an anticharmed baryon opposite a $\overline{p}\Lambda_c^+$ should be suppressed due to the energy required to create four baryons in an event, as well as the small $c\to\Lambda_c$ fragmentation rate. Below is a representation of a sample event in which a $\overline{p}$ and a $\Lambda_c^+ \to pK^-\pi^+$ are observed with a $\overline{D}^0$ or D^- or D_s^- assumed to exist in the opposite hemisphere:

$c \quad \overline{c}$

$\overline{p}\hookleftarrow \qquad \hookrightarrow(\overline{D}^0$ or D^- or $D_s^-)$

$\Lambda_c^+\hookleftarrow \qquad \hookrightarrow$anything

$pK^-\pi^+\hookleftarrow$

After finding the number of S$[\overline{p}\Lambda_c^+]$ events (Fig. 9), we separately find the number of times that a $\overline{p}$ is found opposite a $\overline{D}$. For this double correlation measurement, fully reconstructed mesons are used as the anticharm tag $\overline{D}$. We reconstruct the $\overline{D}^0$ (Fig. 10) through the $K^+\pi^-$ decay mode, the D^- (Fig. 11) through the $K^+\pi^-\pi^-$ decay mode, and the D_s^- (Fig. 12) through the $\phi\pi^-$ decay mode. We require the $\overline{D}$ meson to have momentum $p>2.5$ GeV/c, beyond the maximum possible in $B\to\overline{D}$X events. In these events we assume a Λ_c^+ in the hemisphere opposite the $\overline{D}$.

$c \quad \overline{c}$

$\overline{p}\hookleftarrow \qquad \hookrightarrow\overline{D}^0$ or D^- or D_s^-

$(\Lambda_c^+)\hookleftarrow \qquad \hookrightarrow K^+\pi^-$ or $K^+\pi^-\pi^-$ or $\phi\pi^-$

anything $\hookleftarrow$

Comparing the number of S$[\overline{p}\Lambda_c^+]$ events to the number of O$(\overline{p}|\overline{D})$ events, we are able to calculate $B(\Lambda_c^+\to pK^-\pi^+)$, as follows. First we write an equation for $\mathcal{Y}(\Lambda_c^+)$, the yield of $\Lambda_c^+\to pK^-\pi^+$ events containing a tag antiproton in the same hemisphere of the Λ_c^+:

$$\mathcal{Y}[\Lambda_c^+\overline{p}]=\frac{\mathcal{L}\cdot\sigma(e^+e^-\to c\overline{c})\cdot\mathcal{B}(c\overline{c}\to\overline{p}+\Lambda_c^+ +X+\overline{D}^0 \text{ or } D^- \text{ or } D_s^-)\cdot\mathcal{B}(\Lambda_c^+\to pK^-\pi^+)\cdot\epsilon_{\overline{p}}\cdot\epsilon_{[\Lambda_c^+\overline{p}]}}{1-f_2}, \tag{9}$$

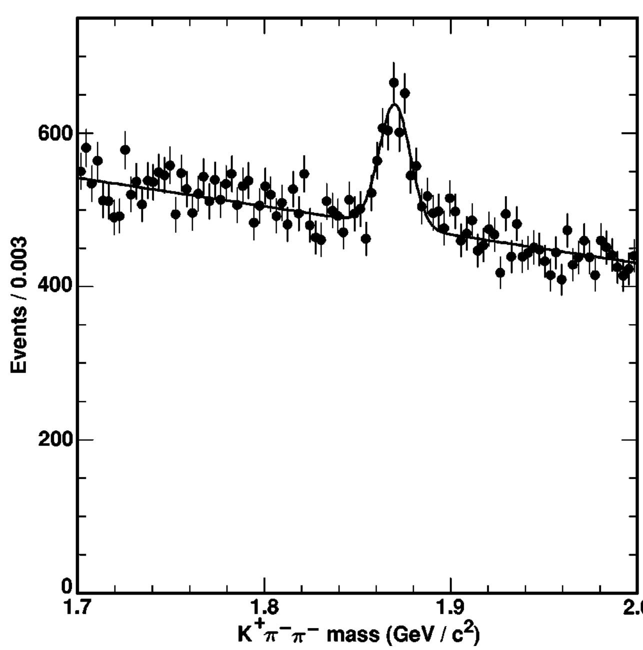

FIG. 11. Candidate D^- mass (i.e., $K^+\pi^-\pi^-$ mass, in GeV/c^2) with a $\overline{p}$ in the opposite hemisphere. In these events a Λ_c^+ is assumed to exist in the hemisphere opposite the D^-: O$(D^-|\Lambda_c^+)$.

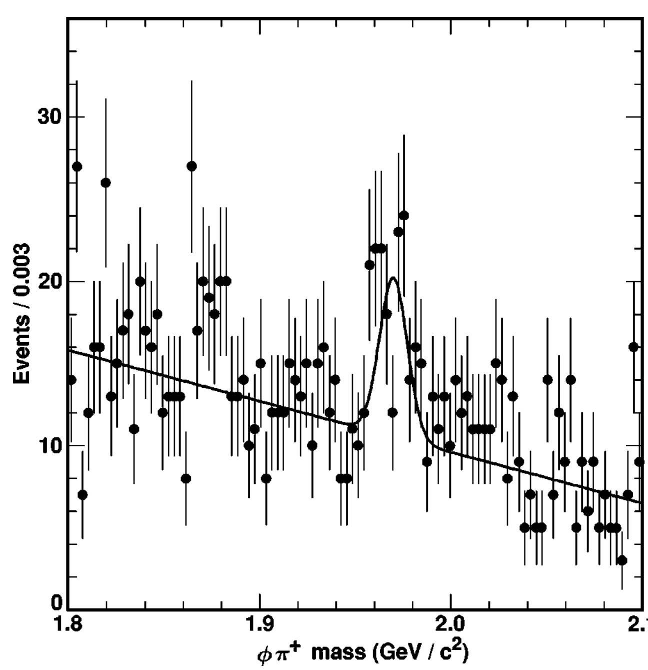

FIG. 12. Candidate D_s^- mass (i.e., $\phi\pi^-$ mass, in GeV/c^2) with a $\overline{p}$ in the opposite hemisphere. In these events a Λ_c^+ is assumed to exist in the hemisphere opposite the D_s^- : O$(D_s^-|\Lambda_c^+)$.

where $\epsilon_{[\Lambda_c^+\overline{p}]}$ is the efficiency for reconstructing a $\Lambda_c^+ \to pK^-\pi^+$ decay in an event containing a tag antiproton and f_2 is defined as the fraction of $\Lambda_c^+\overline{p}$ events not containing a $\overline{D}^0$ or D^- or D_s^-:

$$f_2 \equiv \frac{\mathcal{B}(c\overline{c} \to \overline{p} + \Lambda_c^+ + X' + \text{ anticharmed baryon})}{\mathcal{B}(c\overline{c} \to \overline{p} + \Lambda_c^+ + X)} \tag{10}$$

where the anticharmed baryon could be, e.g., a $\overline{\Lambda}_c$ in which case two baryon pairs must exist in the event.

For $\mathcal{Y}(\overline{D}^0|\overline{p})$, the yield of events containing a $\overline{D}^0 \to K^+\pi^-$ decay in the hemisphere opposite a tag $\overline{p}$, one can write

$$\mathcal{Y}(\overline{D}^0|\overline{p}) = \frac{\mathcal{L} \cdot \sigma(e^+e^- \to c\overline{c}) \cdot \mathcal{B}(c\overline{c} \to \overline{p} + \Lambda_c^+ + \overline{D}^0 + X) \cdot \mathcal{B}(\overline{D}^0 \to K^+\pi^-) \cdot \epsilon_{\overline{p}}^- \cdot \epsilon_{(\overline{D}^0|\overline{p})}}{1 - f_3}, \tag{11}$$

and similarly for $\mathcal{Y}(D^-)$ and $\mathcal{Y}(D_s^-)$, where $\epsilon_{(\overline{D}^0|\overline{p})}$ is the efficiency for reconstructing a $\overline{D}^0 \to K^+\pi^-$ decay in events containing a tag antiproton and where f_3 is defined as the fraction of $(\overline{D}|\overline{p})$ events not containing a Λ_c^+:

$$f_3 \equiv \frac{\mathcal{B}(c\overline{c} \to \overline{p} + \Theta_c' + X' + \overline{D})}{\mathcal{B}(c\overline{c} \to \overline{p} + X + \overline{D})} \tag{12}$$

in which Θ_c' is a charm+baryon system other than a Λ_c^+. The main contributors to the numerator of this equation are events like $e^+e^- \to \overline{D}DN\overline{p}X$ and, to a smaller, negligible extent, events in which a Ξ_c (Sec. IV A 3) is produced. Note that f_3 is closely related to the previously defined f_1 [Eq. (5)]; $f_1 \approx 1 + f_3$.

It then follows that

$$\mathcal{B}(\Lambda_c^+ \to pK^-\pi^+) = \frac{\dfrac{\mathcal{Y}[\Lambda_c^+\overline{p}] \cdot (1 - f_2)}{\epsilon_{[\Lambda_c^+\overline{p}]}}}{\dfrac{\mathcal{Y}(\overline{D}^0|\overline{p}) \cdot (1-f_3)}{\mathcal{B}(\overline{D}^0 \to K^+\pi^-) \cdot \epsilon_{(\overline{D}^0|\overline{p})}} + \dfrac{\mathcal{Y}(D^-|\overline{p}) \cdot (1-f_3)}{\mathcal{B}(D^- \to K^+\pi^-\pi^-) \cdot \epsilon_{(D^-|\overline{p})}} + \dfrac{\mathcal{Y}(D_s^-|\overline{p}) \cdot (1-f_3)}{\mathcal{B}(D_s^- \to \phi\pi^-) \cdot \epsilon_{(Ds^-|\overline{p})}}}, \tag{13}$$

where, as before, particles contained in [ ] are in the same hemisphere with respect to one another and particles contained in ( ) are in opposite hemispheres with respect to one another.

The major contributors to f_2 are events containing $\overline{\Lambda}_c\Lambda_c^+N\overline{p}$. We measure the magnitude of this correction by measuring the yield of events containing a $\overline{\Lambda}_c$ in the hemisphere opposite a tag antiproton. Our equation for f_2 is then

$$f_2 = \frac{\mathcal{Y}(\overline{\Lambda}_c|\overline{p})/\epsilon_{(\overline{\Lambda}_c|\overline{p})}}{\mathcal{Y}[\Lambda_c^+\overline{p}]/\epsilon_{[\Lambda_c^+\overline{p}]}}. \tag{14}$$

The number of $\overline{D}DN\overline{p}$ events are measured using S$[D\overline{p}]$ same hemisphere correlations (Fig. 4; note that the DN combination here is the major component of what we previously referred to as Θ_c'); from these events, we compute f_3:

$$f_3 = \frac{\dfrac{\mathcal{Y}[D^0\overline{p}]}{\epsilon_{[D^0\overline{p}]} \cdot \mathcal{B}(D^0 \to K^-\pi^+)} + \dfrac{\mathcal{Y}[D^+\overline{p}]}{\epsilon_{[D^+\overline{p}]} \cdot \mathcal{B}(D^+ \to K^-\pi^+\pi^+)} + \dfrac{\mathcal{Y}[D_s^+\overline{p}]}{\epsilon_{[D_s^+\overline{p}]} \cdot \mathcal{B}(D_s^+ \to \phi\pi^+)}}{\dfrac{\mathcal{Y}(\overline{D}^0|\overline{p})}{\epsilon_{(\overline{D}^0|\overline{p})} \cdot \mathcal{B}(D^0 \to K^-\pi^+)} + \dfrac{\mathcal{Y}(D^-|\overline{p})}{\epsilon_{(D^-|\overline{p})} \cdot \mathcal{B}(D^+ \to K^-\pi^+\pi^+)} + \dfrac{\mathcal{Y}(D_s^-|\overline{p})}{\epsilon_{(D_s^-|\overline{p})} \cdot \mathcal{B}(D_s^+ \to \phi\pi^+)}}. \tag{15}$$

In this equation, the full expression for $\mathcal{Y}[D^0\overline{p}]$, e.g., is

$$\mathcal{Y}[D^0\overline{p}] = \mathcal{L} \cdot \sigma(e^+e^- \to c\overline{c}) \cdot \mathcal{B}(c\overline{c} \to D^0 + \overline{p} + \Theta_c + X') \cdot \mathcal{B}(D^0 \to K^-\pi^+) \cdot \epsilon_{\overline{p}}^- \cdot \epsilon_{[D^0\overline{p}]}. \tag{15a}$$

TABLE I. Event yields for signal and backgrounds, in data and Monte Carlo simulations. As before, the same hemisphere correlations are designated with brackets [ ], and opposite hemisphere correlations are designated with parentheses ( ). Background yields which are subtracted from the numerator or denominator are indicated with a minus sign.

Double correlations	MC	Data
$\mathcal{Y}[\Lambda_c^+\overline{p}]$ (Numerator)	1656 ± 65	1093 ± 47
$\mathcal{Y}(\overline{D}^0\vert\overline{p})$ (Denominator)	2725 ± 84	1369 ± 55
$\mathcal{Y}(D^-\vert\overline{p})$ (Denominator)	1501 ± 113	963 ± 71
$\mathcal{Y}(D_s^-\vert\overline{p})$ (Denominator)	111 ± 19	51 ± 11
$\epsilon_{\Lambda_c^+}/\epsilon_{D^0}/\epsilon_{D^-}/\epsilon_{D_s^-}$	26.5%/43.7%/32.2%/14.5%	
$\mathcal{Y}(\overline{\Lambda}_c\vert\overline{p})$ (Bkgnd to Num.)	-84 ± 49	-75 ± 39
$\mathcal{Y}[D^0\overline{p}]$ (Bkgnd to Den.)	-268 ± 40	-68 ± 23
$\mathcal{Y}[D^+\overline{p}]$ (Bkgnd to Den.)	-417 ± 67	-152 ± 39
$\mathcal{Y}[D_s^+\overline{p}]$ (Bkgnd to Den.)	-26 ± 11	-1 ± 6
fake $\overline{p}$ in $[D\overline{p}]$ evts. (Bkgnd. to Den.)	-272 ± 31	-298 ± 36
f_2	$(5.1\pm 2.9)\%$	$(6.9\pm 2.2)\%$
f_3 $(\approx f_1 - 1)$	$(17.5\pm 3.4)\%$	$(10.6\pm 2.4)\%$
$\mathcal{B}(\Lambda_c^+ \to pK^-\pi^+)$	4.3% (input)	$(4.9\pm 0.5)\%$
$(\pi^-_{\rm soft}\vert\overline{p})$ Triple correlation		
$\mathcal{Y}(\pi^-_{\rm soft}\vert\overline{p})$ (Denominator)	34222 ± 1092	14553 ± 485
fake $\overline{p}$ in $(\pi^-_{\rm soft}\vert\overline{p})$	-3318 ± 310	-1867 ± 261
$\mathcal{Y}([\Lambda_c^+\overline{p}]\vert\pi^-_{\rm soft})$ (Numerator)	202.8 ± 27.8	101.6 ± 20.6
$\mathcal{B}(\Lambda_c^+ \to pK^-\pi^+)$	4.3% (input)	$(5.2\pm 1.3)\%$
$(e^-\vert\overline{p})$ Triple correlation		
$\mathcal{Y}(e^-\vert\overline{p})$ (Denominator)	4178 ± 65	1739 ± 47
fake $\overline{p}+$ fake e^-	-382 ± 39	-272 ± 41
$\mathcal{Y}([\Lambda_c^+\overline{p}]\vert e^-)$ (Numerator)	20.1 ± 5.2	10.3 ± 3.8
$\mathcal{B}(\Lambda_c^+ \to pK^-\pi^+)$	4.3% (input)	$(5.6\pm 2.5)\%$

B. Estimates of f_2 and f_3

1. f_3 and $D\overline{D}N\overline{p}$ backgrounds

There are two main contributors to f_3: $D\overline{D}N\overline{p}$ events and fake tag antiprotons. They were previously discussed in the Tag identification (Sec. III) and Triple correlation sections (Sec. IV), respectively. Both of these backgrounds inflate the calculated number of $(\overline{D}|\overline{p})$ events [essentially the denominator of $\mathcal{B}(\Lambda_c^+ \to pK^-\pi^+)$, Eq. (13)] and thus will bias us towards a low final result if underestimated in the data. The $D\overline{D}N\overline{p}$ background was found in both data and Monte Carlo simulations using the plots shown in Fig. 4 and a similar one for D_s^-. Monte Carlo simulations give the $\overline{p}$ angular distribution in $DDN\overline{p}$ events. Hence the number of events with D and $\overline{p}$ in the same hemisphere were simply subtracted from the total number of events in the denominator of Eq. (13) for $\mathcal{B}(\Lambda_c^+ \to pK^-\pi^+)$. Numerically, these backgrounds constitute $(17\pm 3)\%$ and $(11\pm 2)\%$ corrections to our initial $(\overline{D}|\overline{p})$ sample in Monte Carlo simulations and data, respectively, as indicated in Table I.

2. f_3 and $\Lambda_c^+\overline{\Lambda}_c N\overline{p}$ backgrounds

There is only one major contributor to f_2, namely $\Lambda_c^+\overline{\Lambda}_c N\overline{p}$ events, as shown in Fig. 13. These events are thought to be rare due to the energy needed to create the four baryons in such an event. However, it is possible that $\overline{\Lambda}_c$ production is enhanced when a Λ_c^+ is produced in an event. In order to estimate this effect we reconstruct events containing a $\overline{p}$ opposite a $\overline{\Lambda}_c$ and assume a charmed baryon opposite the $\overline{\Lambda}_c$ (see Fig. 14). The effect we see is approximately $(7\pm 3)\%$ in data. We, therefore, make an explicit correction of this magnitude (f_2).

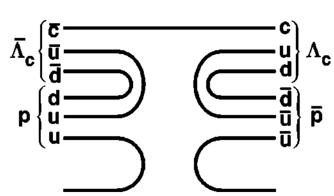

FIG. 13. A possible diagram for producing final states containing four baryons, including a Λ_c opposite a $\overline{\Lambda}_c$.

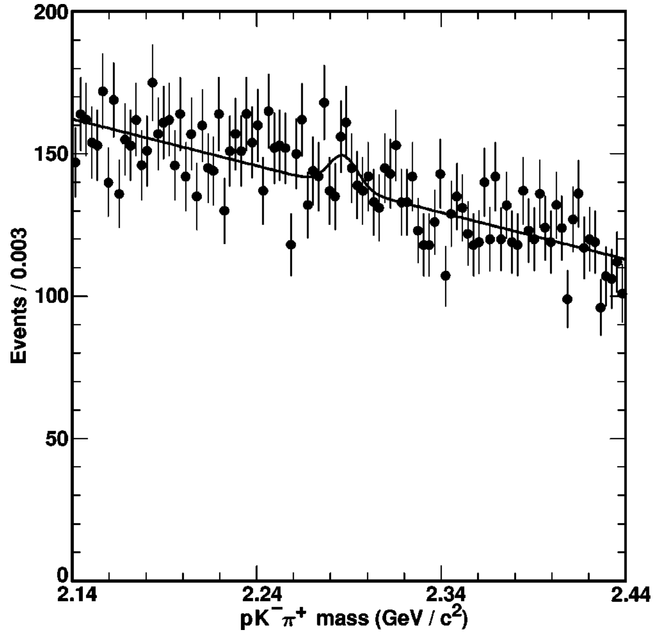

FIG. 14. Candidate $\overline{\Lambda}_c$ mass (i.e., $pK^-\pi^+$ mass, in GeV/c^2) for events containing a $\overline{p}$ in the opposite hemisphere ($\overline{p\Lambda_c}$). The yield of this plot puts an upper limit on $\Lambda_c^+\overline{\Lambda}_cN\overline{p}$ events.

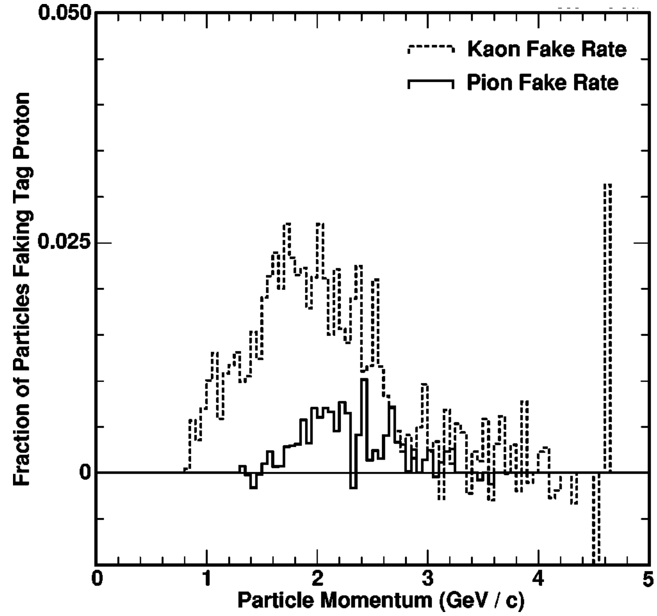

FIG. 15. The percentage of kaons and pions that pass all of our tag proton identification requirements as a function of momentum. The data fake rate was found using kaons and pions from $D^0\to K^-\pi^+$ and $\phi\to K^+K^-$ decays as described in the text.

C. Particle reconstruction efficiency and tag antiproton fakes

In deriving $\mathcal{B}(\Lambda_c^+\to pK^-\pi^+)$, we assume that the Monte Carlo simulation accurately reproduces the efficiency for reconstructing Λ_c^+'s, that is, $\epsilon_{\Lambda_c^+(Data)}=\epsilon_{\Lambda_c^+(MC)}$.

Very approximately, the efficiency for reconstructing a tag antiproton in the $\mathrm{O}(\overline{p}|\overline{D})$-tagged sample should equal the efficiency for reconstructing a tag antiproton in $\mathrm{S}[\overline{p}\Lambda_c^+]$ events. However, the latter sample is obviously biased by the high momentum cut on the Λ_c^+ ($p_{\Lambda_c^+}>2.5$ GeV/c), which forces the same hemisphere antiproton tag into a low momentum regime (the kinematic upper limit on the momentum for a $\overline{p}$ in a signal event to appear colinear with a Λ_c^+ having $p_{\Lambda_c^+}>2.5$ GeV/c is 1.65 GeV/c). In order to restrict the Λ_c^+'s to the same momentum interval in our $\mathrm{O}(\overline{p}|\overline{D})$ sample (denominator) as those in our $\mathrm{S}[\overline{p}\Lambda_c^+]$ sample (numerator), we restrict our calculation of final results to events in which tag antiprotons satisfy the requirement $p_{\overline{\mathrm{p}}}<1.6$ GeV/c. This momentum cut therefore helps ensure that the Λ_c^+ momentum spectrum in the denominator tag sample $\mathrm{O}(\overline{p}|\overline{D})$ is most similar to the Λ_c^+ momentum spectrum in the $\mathrm{S}[\overline{p}\Lambda_c^+]$ sample, which constitutes the numerator in our double correlation ratio.

Below 1.6 GeV/c, we must check that our tag antiprotons in the $\mathrm{O}(\overline{p}|\overline{D})$ sample have the same momentum spectrum as in our $\mathrm{S}[\overline{p}\Lambda_c^+]$ sample. If these subsamples are both drawn from the exact same parent $([\Lambda_c^+\overline{p}]|\overline{D})$ sample, then we certainly expect this to be the case. If the tag antiproton momentum spectrum for our $\mathrm{O}(\overline{p}|\overline{D})$ sample is the same as the tag antiproton momentum spectrum in our $\mathrm{S}[\overline{p}\Lambda_c^+]$ sample, then we are also insensitive to any possible variations in the antiproton-finding efficiency as a function of momentum.

Fake antiprotons can also contaminate our candidate antiproton tag sample, in a momentum-dependent manner. Figure 15 shows the likelihood of a kaon track to fake a proton track as a function of momentum, derived from $\phi\to K^+K^-$ and $D^0\to K^-\pi^+$ events. Note that the rate at which pions fake protons is considerably smaller than the rate at which kaons fake protons (Fig. 15) in the momentum interval of interest ($p<1.6$ GeV/c), since kaons are closer in mass to protons than pions. Since pions tend to have random correlations with both D mesons as well as Λ_c^+'s, pions faking protons largely cancel in both numerator and denominator of Eq. (13). This is not necessarily the case for kaons faking protons.

In $c\overline{c}$ events which do not contain charmed baryons, we expect a D meson recoiling against the tag $\overline{D}$; the D-meson will then decay into a negatively charged kaon $(53\pm4)\%$ of the time if the parent is a D^0 and $(24\pm3)\%$ of the time if the parent is a D^+ [7]. If the parent is a D_s, K^- are produced $(13\pm13)\%$ of the time [7], hence the population of K^- potentially faking $\overline{p}$ is enhanced in our $\overline{D}$-tagged sample. Unfortunately, we have insufficient statistics to determine the level of the fake tag background entirely from data, and we must rely on the Monte Carlo kaon and pion background fractions as a function of momentum to quantify antiproton fakes.

We thus use the following procedure to determine the contribution of fakes to our tag antiproton sample and then extract our final branching fraction:

(1) We plot the tag antiproton momentum spectrum, separately for our $\mathrm{O}(\overline{p}|\overline{D})$ and $\mathrm{S}[\overline{p}\Lambda_c^+]$ samples prior to any corrections (Fig. 16). Since there is some background under

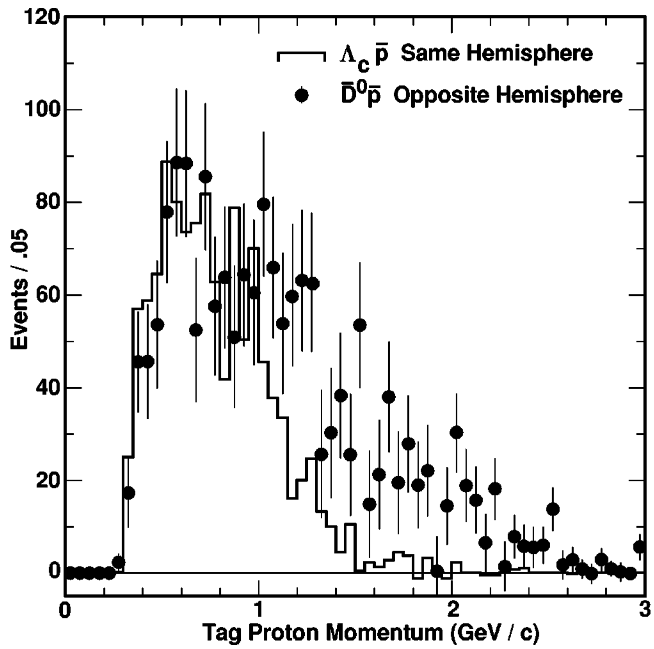

FIG. 16. Data tag antiproton momentum spectrum in $[\Lambda_c^+\overline{p}]$ same hemisphere events (solid histogram) and $\overline{D}$ opposite $\overline{p}$ $\mathrm{O}(\overline{D}|\overline{p})$ events (points) in data, after a sideband subtraction on the Λ_c^+ or $\overline{D}$ mass, prior to subtracting tag antiproton fakes. Notice the excess of high momentum tag antiprotons in the $\mathrm{O}(\overline{D}|\overline{p})$ sample.

the Λ_c^+ and $\overline{D}$ mass distributions, a sideband subtraction must be performed to remove background $(pK^-\pi^+)$-$\overline{p}$ correlations in the case of the $\mathrm{S}[\overline{p}\Lambda_c^+]$ sample, with a similar sideband subtraction for the $\mathrm{O}(\overline{p}|\overline{D})$ sample. The scaled antiproton momentum spectrum opposite $K^+\pi^-$ invariant mass combinations in the $\overline{D}^0$ sidebands $(0.03<|m_{K^+\pi^-}-m_{\overline{D}^0}|<0.1\ \mathrm{GeV})$ is therefore subtracted from the antiproton momentum spectrum opposite $K^+\pi^-$ invariant mass combinations in the $\overline{D}^0$ signal region $(|m_{K^+\pi^-}-m_{\overline{D}^0}|<0.025\ \mathrm{GeV})$. We note in Fig. 16 a large excess above the $p<1.6\ \mathrm{GeV}/c$ kinematic limit, which we attribute, in part, to backgrounds from $D\overline{D}N\overline{p}$ and also kaons producing fake antiproton tags.

(2) We now remove the contribution from non $\overline{pD}\Lambda_c^+$ events (in both data and Monte Carlo simulations) to each of our $\mathrm{O}(\overline{p}|\overline{D})$ and $\mathrm{S}[\overline{p}\Lambda_c^+]$ samples (separately). (a) We first subtract fake antiprotons using the measured kaon-pion fake rates as a function of momentum, multiplied by the kaon and pion production rates as a function of momentum. The per track fake rates are determined directly from data, as described previously. For the production momentum spectra, we rely on Monte Carlo simulations, which are based on the Particle Data Group $D\to K^-X$ exclusive branching fractions and inclusive rates [7]. (b) We additionally subtract contributions due to $D\overline{D}N\overline{p}$ and $\Lambda_c^+\overline{p}N\overline{\Theta}_c$ from the fake-subtracted plot, using data for both of these estimates. These backgrounds are estimated from the yields in Figs. 4 and 14, respectively. The sideband-subtracted antiproton momentum spectra in our $\mathrm{S}[p\overline{D}]$ and $\mathrm{O}(\overline{p}|\overline{\Lambda}_c^-)$ data samples are themselves directly subtracted from the signal $\mathrm{O}(\overline{p}|\overline{D})$ and $\mathrm{S}[\overline{p}\Lambda_c^+]$ antiproton momentum spectra. In doing so, we have removed backgrounds from $D\overline{D}N\overline{p}$ and $\Lambda_c^+\overline{p}N\overline{\Theta}_c$.

After subtracting these backgrounds, we note improved agreement between the data tag antiproton spectrum for the $\mathrm{O}(\overline{p}|\overline{D})$ and $\mathrm{S}[\overline{p}\Lambda_c^+]$ samples (Fig. 17).

(3) After performing the above subtractions, we extract $\mathcal{B}(\Lambda_c^+\to pK^-\pi^+)$, restricting ourselves to the interval where the Monte Carlo and data show good agreement for the $\overline{p}$ momentum spectra $(0.6-1.6\ \mathrm{GeV}/c$; as already mentioned, the upper momentum cut coincides with the kinematically allowed maximum momentum for our tag antiprotons given the minimum momentum requirement on the $\Lambda_c^+)$.

We take a combination of the magnitude of the fake subtraction and the spread in the derived values of $\mathcal{B}(\Lambda_c^+\to pK^-\pi^+)$ when we vary the limits of our tag antiproton momentum acceptance, as an estimate of the systematic error inherent in this procedure ($\sim$15%, Table II).

D. Checks of the $\overline{p}$ momentum spectrum

We have conducted a check of the double correlation analysis by using a sample of events which have the tag antiproton in the opposite (same) hemisphere of (as) the Λ_c^+ $(\overline{D})$, i.e., opposite to the correlation exploited in our standard analysis. Following the above notation, we denote these events as $([\overline{pD}]|\Lambda_c^+)$ events, and the subsample of those events which constitute the denominator and numerator in our double correlation sample as $\mathrm{S}[\overline{pD}]$ and $\mathrm{O}(\overline{p}|\Lambda_c^+)$, respectively. According to JETSET 7.3 simulations, approximately half of all $\overline{pD}\Lambda_c^+$ events will have the antiproton in the same hemisphere as the Λ_c^+ (corresponding to our ''standard'' analysis), with the other half having the antiproton in the opposite hemisphere (see Fig. 8). We do not use these hemisphere-sign correlations in computing $\mathcal{B}(\Lambda_c^+\to pK^-\pi^+)$ for two main reasons—first, the level of $D\overline{D}N\overline{p}$ is much more difficult to determine than for the standard $\mathrm{O}(\overline{p}|\overline{D})$ sample, and second, the $\mathrm{S}[\overline{p}\Lambda_c^+]$ sample is very susceptible to $\overline{\Lambda}_c\Lambda_c^+$ events in which there are no charmed mesons produced—in such a case, the tag antiproton can be a direct decay product of the $\overline{\Lambda}_c$. If we nevertheless trust the Monte Carlo simulations to reproduce all backgrounds and efficiencies for this $\mathrm{S}[\overline{pD}]$-tagged data sample, and calibrate the observed yields in data to Monte Carlo simulations as above in the standard double correlation analysis, we obtain a central value for $\mathcal{B}(\Lambda_c^+\to pK^-\pi^+)$ which differs by $\sim$12% from the standard analysis (see Table II).

This $([\overline{pD}]|\Lambda_c^+)$ sample is much less susceptible to backgrounds from K^- which fake $\overline{p}$ because the D, which would be the putative source of these fakes, is now fully reconstructed. The requirement that the tag antiproton now be found in the $\overline{D}$ hemisphere rather than the Λ_c^+ hemisphere biases the tag antiproton momentum spectrum in a different way than in the ''standard'' analysis. We can thus use these

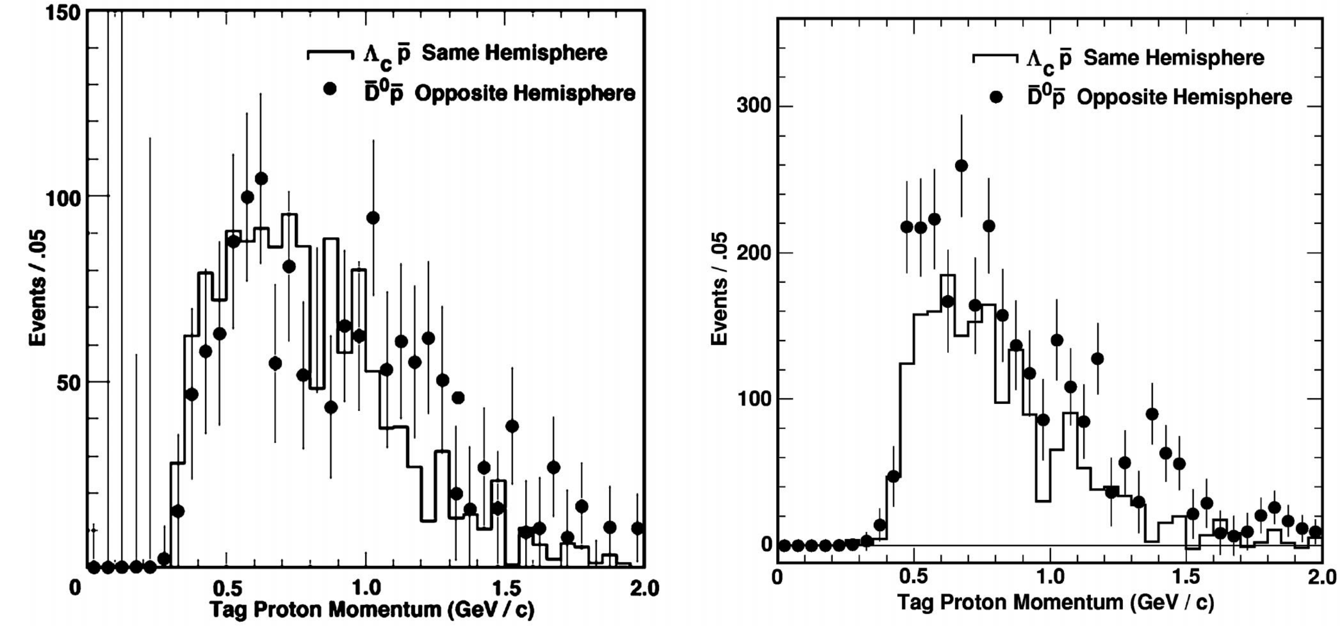

FIG. 17. Left: Previous plot after background subtractions. Tag antiproton momentum in $\Lambda_c^+\overline{p}$ same hemisphere events ($[\Lambda_c^+\overline{p}]$, solid histogram) and $\overline{D}$ opposite $\overline{p}$ events $[\mathrm{O}(\overline{D}|\overline{p}]$, points) in data after a sideband subtraction on the Λ_c^+ or $\overline{D}$ mass, and after subtracting tag antiproton fakes. Right: the corresponding Monte Carlo spectra, after similar subtractions, for comparison.

$(\Lambda_c^+|[\overline{pD}])$ events to qualitatively check our tag $\overline{p}$ momentum spectra in the ''standard'' $([\overline{p}\Lambda_c^+]|\overline{D})$ analysis, after kaon fake subtraction in the standard analysis. The momentum spectrum for tag antiprotons in our cross-check $(\Lambda_c^+|[\overline{pD}])$ sample is shown in Fig. 18. The antiproton momentum spectrum in the $(\Lambda_c^+|[\overline{pD}])$ sample is qualitatively similar to that in the standard $([\Lambda_c^+\overline{p}]|\overline{D})$ analysis, after background corrections.

TABLE II. Summary of systematic errors assessed in measurement of $\mathcal{B}(\Lambda_c^+\to pK^-\pi^+)$.

	π_{soft} tag	Electron tag	Double corr.
Tag proton id/spectrum	15%	15%	15%
Event selection/MC mismodeling	15%	14%	12%
$D\overline{D}N\overline{p}$ background events	8%	8%	8%
Λ_c^+/D momentum spectra	8%	8%	8%
Λ_c^+/D id cuts	5%	5%	5%
Λ_c^+ mass fit/sideband subtraction	6%	10%	1%
Contamination from Σ_c^0, Λ_{cJ}	6%		
Tag electron fakes		5%	
$\Lambda_c^+\overline{\Lambda}_c N\overline{p}$ events			4%
$\mathcal{B}(D^0\to K^-\pi^+)$			2%
$\mathcal{B}(D^+\to K^-\pi^+\pi^+)$			3%
Beam-wall/Beam-gas contamination	3.5%	3.5%	3.5%
Contamination of Ξ_c, Ω_c events	3%	3%	3%
Hemisphere correlation	2%	2%	2%
Total	28%	25%	24%

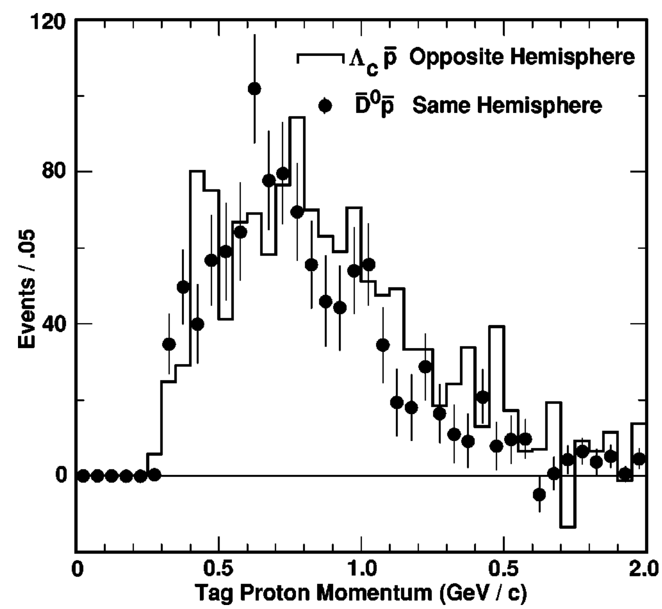

FIG. 18. Cross-check results. Tag antiproton momentum in $\mathrm{O}(\Lambda_c^+|\overline{p})$ opposite hemisphere events (solid histogram) and $\mathrm{S}[\overline{Dp}]$ same hemisphere events (points) in data, after a sideband subtraction on the Λ_c^+ or $\overline{D}^0$ mass. This sample should be less susceptible to tag proton fakes, since the sign correlation is not correct for kaons coming from semileptonic charm decay to fake antiprotons, as was the case for our $\overline{D}$ opposite $\overline{p}$ event sample. However, we do not use these hemisphere-sign correlations in computing $\mathcal{B}(\Lambda_c^+\to pK^-\pi^+)$ due to the difficulty in estimating the $D\overline{D}N\overline{p}$ and $\Lambda_c^+\overline{\Lambda}_c$ backgrounds in this event sample.

VI. RESULTS

Our results, showing the yields $\mathcal{Y}$, efficiencies ϵ, and backgrounds, in both data and Monte Carlo simulations, are tabulated in Table I. The weighted average of the three techniques corresponds to $\mathcal{B}(\Lambda_c^+ \to pK^-\pi^+) = (5.0 \pm 0.5)\%$ (statistical error only).

VII. SUMMARY OF SYSTEMATIC UNCERTAINTIES

We have already discussed many of the systematic errors and their assessment in previous sections. Table II lists the systematic errors evaluated for the three methods of extracting $\mathcal{B}(\Lambda_c^+ \to pK^-\pi^+)$. As discussed previously, the largest systematic error is due to uncertainties in the tagging efficiency and spectrum. This includes possible backgrounds to the antiproton tags, and the difference between the $\bar{p}$ momentum spectra in S$[\Lambda_c \bar{p}]$ and O$(\bar{D}|\bar{p})$ events. Uncertainties in backgrounds and tagging efficiencies are assessed, in part, by varying the tag antiproton momentum interval over which our final result is extracted by ± 300 MeV/c in either direction from the default value. The error (''Event selection/MC mismodeling'') is evaluated by varying the event selection criteria for both data and Monte Carlo simulations and determining the variation in the calculated final result. This error also includes the discrepancy between the central value we quote and the result obtained from the cross check in which the antiproton is identified in the same hemisphere as the charm tag. It also includes the variation in the final result obtained using different versions of charged track reconstruction software, comparing the internal consistency of different data subsamples, and different versions of the Monte Carlo event generator and detector simulation.

VIII. DISCUSSION AND CONCLUSIONS

Employing new techniques of baryon-charmed particle correlations in $e^+e^- \to c\bar{c}$ annihilations at a center-of-mass energy $\sqrt{s} \sim 10.55$ GeV, we measure $\mathcal{B}(\Lambda_c^+ \to pK^-\pi^+) = (5.0 \pm 0.5 \pm 1.2)\%$. At present, this technique is limited by our understanding of the nonsignal backgrounds (most notably, $D\bar{D}N\bar{p}$ backgrounds); presumably, more data would allow a greater understanding of those backgrounds. Our result is consistent with the determination of $\mathcal{B}(\Lambda_c^+ \to pK^-\pi^+) = 7 \pm 2\%$ suggested by Dunietz [6], based on the measured ratio for $\mathcal{B}(\Lambda_c^+ \to \Lambda X l \nu)/\mathcal{B}(\Lambda_c^+ \to pK^-\pi^+)$ and assuming that the semileptonic charmed baryon width is the same as the semileptonic charmed meson width. It is also consistent with the value of $(5.0 \pm 1.3)\%$ derived by the Particle Data Group [7]. We now discuss the implications of this result and its consistency with related measurements.

The product branching fraction: $\mathcal{B}[B \to (\Lambda_c^+ X$ or $\bar{\Lambda}_c X)] \cdot \mathcal{B}(\Lambda_c^+ \to pK^-\pi^+)$ can be directly determined by simply measuring the efficiency-corrected $\Lambda_c^+ \to pK^-\pi^+$ yield in $B\bar{B}$ events. An unpublished CLEO result finds a value of $\mathcal{B}[(B+\bar{B}) \to \Lambda_c^+] \cdot (\Lambda_c^+ \to pK^-\pi^+) = (1.81 \pm 0.22 \pm 0.24) \times 10^{-3}$ [16] for this product branching fraction. Given that, $\mathcal{B}(\Lambda_c^+ \to pK^-\pi^+) = 0.05$ implies that $\mathcal{B}[B \to (\Lambda_c^+ \; or \; \bar{\Lambda}_c)] \sim 3.6\%$. This can be compared to the Particle Data Group value of $\mathcal{B}(B \to p$ or $\bar{p}) \sim 8.0\%$ [7]. Our result therefore implies that $B \to baryons$ may be occurring at a substantial rate through modes such as $\bar{B} \to DN\bar{N}$X [17], $\bar{B} \to \Xi_c \bar{Y}$X, or $\bar{B} \to \Xi_c \bar{\Lambda}_c$. CLEO has recently published evidence for the latter modes [18].

We can also place bounds on the $\Lambda_c^+ \to pK^-\pi^+$ branching fraction by using the measured CLEO $e^+e^- \to$ hadrons cross section, assuming that the $c\bar{c}$ fraction is 40% of the total hadronic cross section. CLEO has measured $\mathcal{B}(\Lambda_c^+ \to pK^-\pi^+) \cdot \sigma[e^+e^- \to (\Lambda_c^+ + \bar{\Lambda}_c)] = 10 \pm 1$ pb. That measurement simply determines the total yield of either Λ_c^+ or $\bar{\Lambda}_c$ in e^+e^- annihilations; i.e., it determines the sum of $c \to \Lambda_c^+$ plus $\bar{c} \to \bar{\Lambda}_c$. Our value of $\mathcal{B}(\Lambda_c^+ \to pK^-\pi^+) = 0.05$ implies that $\sigma[e^+e^- \to (\Lambda_c^+ + \bar{\Lambda}_c)] = 200$ pb. Using the recent CLEO measurement of $R \equiv \sigma(e^+e^- \to q\bar{q})/\sigma(e^+e^- \to \mu^+\mu^-)$ [19], which corresponds to a value of $\sigma(e^+e^- \to q\bar{q}) \sim 3.3$ nb, and using the JETSET value of $c \to \Lambda_c^+ \sim 0.07$, we have $\sigma(e^+e^- \to q\bar{q}) \times c\bar{c}/q\bar{q} \times (c \to \Lambda_c^+ + \bar{c} \to \bar{\Lambda}_c) = 3300 \text{ pb} \times 0.4 \times 0.07 \times 2 = 185$ pb, in good agreement with our measurement above.

Finally, since the presently tabulated exclusive Λ_c^+ decays are all normalized to $\mathcal{B}(\Lambda_c^+ \to pK^-\pi^+)$, we conclude that $\sim 50\%$ of the Λ_c^+ width is unaccounted for. Since the Λ_c^+ lifetime is only $\sim 40\%$ of the D^0/D_s lifetime, it has long been realized that diagrams such as exchange diagrams, and/or final states including neutrons, are likely to be large contributors to Λ_c^+ decay and may produce final states different than the ''usual'' states expected from simple $\Lambda_c^+ \to \Lambda W_{\text{external}}$ diagrams. Measurement of such decays await additional data and analysis.

ACKNOWLEDGMENTS

We gratefully acknowledge the effort of the CESR staff in providing us with excellent luminosity and running conditions. J.R. Patterson and I.P.J. Shipsey thank the NYI program of the NSF, M. Selen thanks the PFF program of the NSF, M. Selen and H. Yamamoto thank the OJI program of DOE, J.R. Patterson, K. Honscheid, M. Selen, and V. Sharma thank the A.P. Sloan Foundation, M. Selen and V. Sharma thank the Research Corporation, F. Blanc thanks the Swiss National Science Foundation, and H. Schwarthoff and E. von Toerne thank the Alexander von Humboldt Stiftung for support. This work was supported by the National Science Foundation, the U.S. Department of Energy, and the Natural Sciences and Engineering Research Council of Canada.

[1] The ARGUS Collaboration, H. Albrecht *et al.*, Phys. Lett. B **269**, 234 (1991).
[2] The CLEO Collaboration, T. Bergfeld *et al.*, Phys. Lett. B **323**, 219 (1994).
[3] M. A. Ivanov *et al.*, Phys. Lett. B **467**, 58 (2000).
[4] The CLEO Collaboration, G. Crawford *et al.*, Phys. Rev. D **45**, 752 (1992); M. Procario *et al.*, Phys. Rev. Lett. **73**, 1472 (1994).
[5] The ARGUS Collaboration, H. Albrecht *et al.*, Z. Phys. C **58**, 191 (1993); **42**, 191 (1989).
[6] I. Dunietz, Phys. Rev. D **58**, 094010 (1998).
[7] Particle Data Group, C. Caso *et al.*, Eur. Phys. J. C **3**, 1 (1998).
[8] The CLEO Collaboration, R. Ammar *et al.*, Phys. Rev. D **55**, 13 (1997).
[9] The CLEO Collaboration, Y. Kubota *et al.*, Nucl. Instrum. Methods Phys. Res. A **320**, 66 (1992).
[10] G. Fox and S. Wolfram, Phys. Rev. Lett. **41**, 1581 (1978).
[11] G. Crawford *et al.*, Nucl. Instrum. Methods Phys. Res. A **345**, 429 (1994).
[12] S. Brandt and H.D. Dahmen, Z. Phys. C **1**, 61 (1979).
[13] The CLEO Collaboration, D. Akerib *et al.*, Phys. Rev. Lett. **71**, 3070 (1993).
[14] JETSET 7.3: T. Sjöstrand and M. Bengtsson, Comput. Phys. Commun. **43**, 367 (1987).
[15] R. Brun *et al.*, GEANT 3 *Users Guide*, CERN DD/EE/84-1 (1987).
[16] M. Zoeller, Ph.D. thesis, State University of New York, Albany, 1994.
[17] I. Dunietz, FERMILAB-CONF-97-230-T, hep-ph/9708252; Proceedings of the 2nd International Conference on B physics and CP violation, Honolulu, Hawaii, 1997.
[18] The CLEO Collaboration, B. Barish *et al.*, Phys. Rev. Lett. **79**, 3599 (1997).
[19] The CLEO Collaboration, R. Ammar *et al.*, Phys. Rev. D **57**, 1350 (1998). The cross section quoted here is, of course, approximate since we do not specify the infrared cutoff for initial-state radiation.